

1 **Development of a Mississippian–Lower Pennsylvanian isolated carbonate platform**
2 **within the basinal griottes facies of the Cantabrian Mountains, NW Spain**

3

4 **S. Blanco-Ferrera^{1*}, P. Cózar², J. Sanz-López¹**

5

6 ¹Department of Geology, Faculty of Geology, University of Oviedo, c/ Jesús Arias de
7 Velasco s/n, 33005 Oviedo, Spain

8 ²Instituto de Geociencias (CSIC-UCM), Ciudad Universitaria, 28040 Madrid, Spain

9

10 * Corresponding Author. Silvia Blanco-Ferrera

11

12 Silvia Blanco-Ferrera 0000-0001-6255-4322

13 Pedro Cózar 0000-0002-4669-8702

14 Javier Sanz-López 0000-0002-1619-1214

15

16

17 **Abstract**

18 The Valdediezma platform consists of upper Tournaisian to lower Bashkirian
19 (Carboniferous) shallow-water carbonates deposited in the core of the Picos de Europa
20 Province (Cantabrian Mountains, northwest Spain). Although faulted in several thrust
21 sheets, it is the only preserved platform developed in the Mississippian starved basins of
22 the southern branch of the Variscan Orogen that is characterized also by pelagic
23 sedimentation. This unusual platform provides an exceptional opportunity to study the
24 lateral variation from the platform to the typical condensed griotte limestones developed
25 in a starved basin, the origin of such a platform in a particularly unfavourable setting for
26 carbonate accumulation, as well as the nucleation of the subsequent widespread
27 Pennsylvanian carbonate platforms of the Cantabrian Mountains. Sixteen carbonate
28 microfacies are differentiated in the Valdediezma Limestone, from shallow-water to
29 slope to basinal environments. The carbonate production is related to the submarine
30 topography and the rapid rates of microbial mound growth and accumulation,
31 particularly from the upper Viséan to the lower Serpukhovian. A high-elevation
32 platform and steep southern margin occurred during the deposition of condensed
33 cephalopod-bearing limestones in the basin. A higher rate of carbonate accumulation is
34 recognized from the upper Serpukhovian and younger, with similar thicknesses in
35 shallow- and deeper-water settings. The thickest part of the succession was coeval with
36 the larger subsidence resulting from the migration of the Variscan deformation at the
37 margin of the foreland basin of the Cantabrian Zone. The migration of deformation
38 along the foreland uplifted the Valdediezma platform from the lower Bashkirian and
39 caused its partial erosion. The Pennsylvanian carbonate platform developed on an
40 exhumed Mississippian platform. Tectonic overloading due to the emplacement of

41 nearby thrust sheets caused the subsidence and burial of the Valdediezma platform in
42 the upper Moscovian.

43

44 **Keywords** carbonates, microbial boundstones, Carboniferous, Variscan Orogen

45

46 **Declarations**

47 **Funding.** This research was supported by the project CGL2016-78738 of the Spanish
48 Ministry of Research and Innovation.

49 **Declaration of competing interest.** The authors declare that they have no known
50 competing financial interests or personal relationships that could have appeared to
51 influence the work reported in this paper.

52 **Availability of material.** All the thin sections used in the study are housed in the P.

53 Cózar's collection of the Universidad Complutense de Madrid. Conodont specimens are
54 housed in the collection of the Museum of Geology of the University of Oviedo.

55 **Acknowledgements.** Early comments and improvement of the English by G.

56 Sevastopulo, I.D. Somerville, M.W. Hounslow and G. Della Porta are acknowledged.

57 We thank two anonymous reviewers for their constructive comments. Thanks to the

58 collaboration of the Picos de Europa National Park, field works were possible.

59

60 **Introduction**

61

62 Mississippian rocks of the Cantabrian Zone (CZ; Fig. 1) have been rarely studied from a
63 sedimentological aspect due to the predominantly pelagic to hemipelagic settings during
64 the late Tournaisian–late Serpukhovian, represented by the Alba Formation (Eichmüller
65 and Seibert 1984; Wendt and Aigner 1985; Fig. 2a). Breccias, debris flow and slump
66 deposits have been rarely described in these units, and their occurrence was generally
67 associated with the margins of sedimentary highs where condensed cephalopod-bearing
68 limestones were deposited (Eichmüller and Seibert 1984). Higher up in the succession,
69 during the upper Serpukhovian to lower Bashkirian, laminated limestones of the
70 Barcaliente Formation were deposited in a moderately-deep basin of the foreland
71 margin. Siliciclastic turbidite deposits filled the foredeep on the western margin of the
72 CZ, which were transported from the hinterland to the west (Reuther 1977; Oliveira et
73 al. 2019). Mississippian pelagic nodular cephalopod-bearing limestones (such as those
74 of the Alba Formation) widely occur in the southern branch of the Variscan chain in
75 southern Europe, below younger limestones equivalent to the Barcaliente Formation
76 and/or coeval siliciclastic deposits (Pyrenees, Betics, Montagne Noire, Southern Alps
77 and Graz, and the Balkan Peninsula; Schönlaub and Histon 2000; Sudar et al. 2018).

78 Recently, Viséan to lower Bashkirian shallow-water carbonates have been
79 discovered in the core of the Picos de Europa Province (CZ; Figs. 1, 2a), informally
80 named as the Valdediezma Limestone (Sanz-López et al. 2018). The morphology and
81 development of the platform remained poorly explored to date. Intact Mississippian
82 shallow-water platforms are not preserved in the southern branch of the Variscan belt,
83 where original carbonate platforms were eroded and reworked into younger synorogenic
84 siliciclastic deposits (e.g., Engel et al. 1981; Oliveira et al. 2019). Thus, the

85 Valdediezma platform constitutes an exceptional record of a shallow-water platform in
86 this part of the Variscan Orogen, an area that was largely dominated by pelagic and
87 hemipelagic sedimentation.

88 Scant knowledge of Mississippian shallow-water carbonates contrasts with the
89 excellent exposures of the Pennsylvanian carbonate facies and its geometric spatial
90 relations to mapped shallow-water platforms and basinal facies (e.g., Bahamonde et al.
91 1997, 2007, 2008; Della Porta et al. 2002, 2004; Merino-Tomé et al. 2009, 2014). The
92 rocks of the Mississippian-early Bashkirian Valdediezma platform were misinterpreted
93 as Moscovian platform-top facies (Bahamonde et al. 2007, figs. 8C, 13). Moreover, the
94 Valdediezma Limestone was also confused with the Barcaliente, Valdeteja and most of
95 the Picos de Europa formations in regional maps of the central-eastern part of the Picos
96 de Europa Province (Fig. 2) (Merino-Tomé et al. 2014; and previous maps). Thick
97 amalgamations of rather similar massive pale grey limestones occur in those units, and
98 only the biostratigraphy provided by microfossils allows a subdivision of the
99 stratigraphic succession (e.g., Blanco-Ferrera et al. 2017; Sanz-López et al. 2018).

100 We describe a new shallow-water carbonate platform set within the context of
101 deeper-water facies which has been overlooked for decades by the vast Pennsylvanian
102 platform of the Cantabrian Mountains. We demonstrate that this platform was the seed
103 for the Pennsylvanian platform development, a new mechanism not hinted at so far. The
104 aims of this study are: (i) to characterize the lithostratigraphy and sedimentology of the
105 only existing platform laterally interbedded with the deep-water and condensed griotte
106 facies in the southern Variscan front for the Mississippian and basal Pennsylvanian; (ii)
107 to reconstruct and correlate the shallow-water carbonate platform, the platform slope
108 and the transition to the basinal settings using a detailed biostratigraphy; (iii) to discuss
109 the mechanisms for the onset of the shallow-water facies within the dominant pelagic

110 and hemipelagic environments (such mechanism for the rest of the southern Variscan
111 front has been rarely discussed because the shallow-water limestones were mostly
112 reworked in Pennsylvanian synorogenic flysch); (iv) to characterize the regional
113 tectonic factors controlling the demise of the platform and its relationship with the
114 younger Pennsylvanian platform, set within the context of the foreland of the southern
115 branch of the Variscan Belt.

116

117 **Geological context**

118

119 The Cantabrian Zone (CZ) is a tectonostratigraphic unit situated in the northwestern
120 part of the Iberian massif (Fig. 1) and consists of a foreland basin system in the
121 southeastern external part of the Variscan Belt. It contains a thick Palaeozoic succession
122 that was deformed by thin-skinned tectonics (folds and thrusts) during the Variscan
123 Orogeny (Pérez-Estaún et al. 1988). Six tectono-stratigraphic provinces have been
124 defined in the CZ (Julivert 1971, 1978): the Narcea thrust sheets, the Fold and Nappe
125 Province (Somiedo, Esla, Valsurbio, Bodón y Aramo units), the Central Coal Basin (or
126 Asturian Coalfield), the Ponga Nappe, the Picos de Europa and the Pisuerga-Carrión
127 provinces (Fig. 1). The studied area is in the Tejo tectonic unit which is situated in the
128 central-eastern part of the Picos de Europa Province (Fig. 2b). It constitutes part of the
129 northern branch of the Asturian Arc, and its tectonic style has been described as an
130 imbricate system of thrust sheets stacked from the north during the late Moscovian–
131 Gzhelian time interval (Marquínez 1989; Farias and Heredia 1994; Merino-Tomé et al.
132 2009).

133 The Tejo unit includes the most extensive outcrops of the Valdediezma Limestone. It
134 is bounded by the Tresviso (or Cabuérniga) Fault to the north and the San Carlos and

135 Saigu faults to the south (Fig. 2b). The San Carlos Fault is a Variscan thrust rotated as a
136 subvertical fault that results in a triangular-shaped outcrop of the Tejo unit. The San
137 Carlos Fault (like the Cabañes Fault to the northeast) has a long movement history and
138 controlled Permian and Mesozoic sedimentation. These faults subsequently experienced
139 reverse displacements during the Alpine Orogeny (Espina 1994). Triassic strata are
140 locally preserved in the footwall of the Tresviso reverse Fault (Fig. 2b).

141 The Tejo unit consists of several tectonic subunits bounded by faults, which, from
142 northwest to the southeast, are the Saigu, Varera, Las Llamas-Bejes, La Hermida and
143 the Mesa Sin Pan subunits (Fig. 2b). The Valdediezma Limestone was only informally
144 described because its lower boundary corresponds to faults in the different tectonic
145 subunits. The top of the Valdediezma Limestone is an erosive surface situated below
146 latest Moscovian–Kasimovian strata of the uppermost part of the Picos de Europa
147 Formation (Fig. 2a). Locally, Kasimovian shales and limestones of the Aliva and the
148 Las Llacerias formations directly overlie the Valdediezma Limestone (and in places,
149 continental Permian and Triassic rocks; Sanz-López et al. 2018). The Valdediezma
150 Limestone is exposed below the Barcaliente Formation only in the Mesa Sin Pan
151 subunit.

152 Outcrops located to the north of the Tejo unit (Gamonedo-Cabrales thrust unit; Fig.
153 2b), and south and west (Aliseda-Cabrones-Vegas de Sotres thrust unit, ACVS) are
154 represented by the typical lithostratigraphic succession of upper Tournaisian to
155 Moscovian of the CZ (Fig. 2a). These are the Alba, Barcaliente, Valdeteja and Picos de
156 Europa formations (e.g., Colmenero et al. 2002). Only in outcrops of the ACVS
157 Serpukhovian strata of the Valdediezma Limestone is sandwiched between the Alba and
158 Barcaliente formations (Fig. 2a). Microfossils from the Valdediezma Limestone support
159 the correlation to both these formations (Sanz-López et al. 2018).

160

161 **Materials and methods**

162

163 A field survey in the region allowed us to distinguish the main tectonic subunits, from
164 which eleven stratigraphic sections have been measured. These sections are the most
165 representative and contain the entire diversity of recognized facies (Fig. 2b). The
166 sampling interval was not uniform, but varies typically, between 2 to 4 m, but can be up
167 to 10 metre intervals (depending on the observed facies) in sections several hundred
168 metres-thick, containing the thickest and most representative succession of the platform
169 (e.g., Valdediezma valley and Jitu l'Escarandi sections). A sampling interval of a few
170 centimetres was used on condensed carbonate sections, where the entire section is only
171 10 metres thick (e.g., Vegas de Sotres section). In total, 490 samples were collected in
172 the main sections, as well as some spot samples (about 100) in other studied sections.
173 More than 3000 thin sections (28 x 48 mm) were prepared for microfacies analysis.
174 Classifications by Dunham (1962), Embry and Klovan (1971), Wright (1992) and
175 Rodríguez-Martínez et al. (2010) were used to describe the microfacies. The abundance
176 of grains, cement and matrix was visually estimated using the charts of Baccelle and
177 Bosellini (1965).

178 Foraminifers were studied in 3000 thin sections for ascertaining biostratigraphy.
179 Additionally, 170 samples of 2–11 kg were collected and processed for conodonts. The
180 detailed biostratigraphy was published in Cózar et al. (2015, 2016, 2018a), Blanco-
181 Ferrera et al. (2017) and Sanz-López et al. (2018). The microfossil analysis allowed a
182 subdivision of the succession largely ranging from Mikhailovian (late Viséan) to a
183 probable Krasnopolyanian (early Bashkirian) age according to Cózar et al. (2018a).

184 Correlations with the regional Russian substages from the Moscow Basin follow the
185 nomenclature used in Davydov et al. (2012, fig. 23.1).

186

187 **Facies distribution and environmental interpretation**

188

189 Lithological variations have been grouped in a total of 16 microfacies (Facies F1-F16),
190 which are summarized in Table 1, and displayed in the different tectonic subunits and
191 stratigraphic sections in Figs. 3 to 7.

192

193 **Saigu subunit**

194 Compared to the other tectonic subunits, the Saigu subunit shows a significant
195 contribution of microbially-induced facies, mainly formed during the upper Viséan (Fig.
196 3). This subunit is entirely composed of the Valdediezma Limestone, and no other
197 Mississippian aged formations are recognized within the succession. However, the
198 vertical distribution of facies through the succession allows a subdivision into seven
199 intervals, dependent on the predominant microfacies (numbered as I1 to I7 in Fig. 3). In
200 the lower I1 interval of the Valdediezma valley and coinciding with rocks assigned to
201 the Mikhailovian Substage (Viséan), there is a predominance of cementstone (sensu
202 Wright 1992), as well as peloidal cement- and matrix supported facies (sensu
203 Rodríguez-Martínez et al. 2010) (Facies F1 to F3 in Table 1; Fig. 3a), alternating with
204 bioclastic cement-supported limestones (Facies F5; Fig. 3b–c). Rudstones (Facies F15)
205 are composed of micropeloidal pebbles. Mudstone and wackestone textures (Facies F8;
206 Fig. 3f) have negligible abundance. The most common bioclasts are crinoids, followed
207 by fenestellid bryozoans and brachiopods. Other bioclasts are scarce and sparsely
208 distributed. Facies with fenestrae filled with radiaxial fibrous cement (RFC) (e.g.,

209 Richter et al. 2011) and blocky cement (BC) (e.g., Flügel 2004) are common (Fig. 3a–
210 b). Foraminifers and cyanobacteria (mostly *Girvanella* and *Ortonella*) occur sparsely.
211 At outcrop, it is difficult to recognize morphological differences in the strata due to
212 weathering of the limestone surface. Small domed-shaped morphologies are locally
213 developed that are 8 to 20 m high and laterally extend over less than 100 m (Fig. 4a–b).

214 Higher up in the succession (interval I2) and during most of the Venevian (Viséan),
215 the prevailing lithofacies are like the previous interval (Facies F1–F3). A single
216 bioclastic cement-supported bed (Facies F5) and rudstone bed (Facies F16) occurs (Fig.
217 3). Skeletal remnants of fenestellid bryozoans predominate over brachiopods and
218 crinoids. However, foraminifers are relatively common as well as cyanobacteria,
219 Aphralysiacean, problematic Algospongia (*Claracrusta*, *Ungdarella*, *Falsocalcifolium*
220 and *Praedonezella*; see Vachard and Cózar 2010, for the suprageneric classification of
221 the Algospongia documented in this study), as well as the problematic bryopsidal green
222 alga *Saccamminopsis*. The bedding morphology of the limestones is poorly observed,
223 although the size of mounds may be larger than in the underlying interval, because
224 bedding is not easily recognized in many intervals up to 50 m thick.

225 During the Venevian and most of the Tarussian (Viséan-Serpukhovian), the
226 predominant lithofacies of the interval I3 (Fig. 3) is similar to those at the base of the
227 section, with common cementstone and peloidal lithofacies (Facies F1–F3), alternating
228 with bioclastic cement- and matrix-supported facies (Facies F5–F6; Fig. 3C). Crinoids
229 are abundant, although brachiopods are the predominant skeletal component in some
230 beds. Foraminifers are common, as well as fenestellids and the Algospongia
231 *Praedonezella* as the main skeleton-rigid bioconstructor. Rudstones are only present in
232 the lower Tarussian. Individual dome-shaped morphologies of lithosomes are
233 recognized but are smaller than at the base of the section (domes less than 10 m thick,

234 with lateral extensions of some tens of metres). Ooidal grainstone facies occur rarely
235 (Facies F14; Fig. 3h).

236 The interval from the upper part of the Tarussian to the lower part of the Protvian
237 (Serpukhovian; interval I4) is marked by a sharp change in the lithology and
238 components. This change is highlighted by: (i) rare cementstone and peloidal-
239 micropeloidal cement-supported facies (Facies F1-F4), compared to the underlying
240 intervals; (ii) predominance of bioclastic cement- and matrix-supported facies (Facies
241 F5-F6); (iii) rudstones are composed of bioclastic and/or oolitic pebbles (Facies F16);
242 (iv) abundant grainstone beds (Facies F13-14; Fig. 3g-h), including oolitic grainstones;
243 (v) abundant and diverse green algae (e.g., *Eovelebitella*, *Anatolipora*, *Borladella*,
244 *Paraepimastopora*, *Cabrieroporellopsis* and *Atractyliopsis*; see Vachard et al. 2016 for
245 the systematics of this group). In this interval, the cementstone and micropeloidal
246 textures are commonly capped by grainstone facies.

247 During most of the Protvian (interval I5 in Fig. 3), the facies returned to the
248 previously predominant peloidal-bioclastic carbonate microfacies (Facies F5-F6), with
249 rare mudstone, wackestone (Facies F7 and F9) and rudstones (composed of
250 micropeloidal clasts; Facies F15). Individual morphology of lenses that display dome-
251 shaped bodies are recognized in coalesced associations (interval I5 in Fig. 4c). In
252 contrast to the lower part of the section, they are rich in bioclasts, which mostly includes
253 *Algospongia Calcifolium*, *Praedonezella* and *Fasciella*. Dasycladal green algae occur,
254 and foraminifers are relatively abundant. The abundance of *Calcifolium* increases
255 upwards, but only in the uppermost samples does it constitute 20-30% by volume,
256 values typically present in the overlying interval.

257 The succeeding interval I6 represents most of the Zapaltjubian and it is mainly
258 characterized by: (i) poorly developed microbial facies (bioclastic, as well as peloidal-

259 micropeloidal); (ii) abundant bioclastic packstones and grainstones (Facies F10, F13);
260 (iii) abundant *Calcifolium* (up to 45% of the facies by volume); and (iv) highly diverse
261 bioclastic content.

262 The carbonates of the uppermost Zapaltjubian and Voznesenian
263 (Serpukhovian/Bashkirian boundary interval) contain abundant diagenetic chert nodules
264 (interval I7 in Fig. 3). They indicate another distinct change in sedimentation style
265 shown by: (i) rare microbial strata; (ii) a predominance of mudstones to wackestones;
266 (iii) rather diverse bioclastic content ; (iv) an abundance of calcispheres (mostly in the
267 lower half); (v) the lower half is also characterized by the large accumulations of small
268 mounds (boundstones) of *Calcifolium/Praedonezella*, which are replaced by *Donezella*
269 in the upper part; (vi), mudstones commonly show lumpy texture, possibly related to
270 cyanobacteria influence (although calcified cyanobacteria filaments are rarely
271 recognized); and (vii) the occurrence of packstone beds is rare.

272 The upper part of the Valdediezma Formation shows brecciated levels with mud-
273 cracks and pedotubules in limestones near Jitu l'Escarandi, as well as in the Tresviso
274 area. Palaeosols *sensu stricto* containing clays have not been recognized. The brecciated
275 levels occur 20 m below the breccia that separates the Valdediezma Limestone from the
276 Triassic red beds in the Jitu l'Escarandi section. In the Cheese Cave area (Sobra Valley),
277 grainstones of *Penella* with superficial ooidal coatings (interpreted as spores of green
278 algae by Flügel 2004), typical ooidal grainstones, and one coral horizon occur in the
279 uppermost interval (60–80 m thick). This interval was considered as possibly
280 Krasnopolyanian in age (early Bashkirian) according to Cózar et al. (2018a).

281

282 *Interpretation.*— The lower interval I1 (Mikhailovian) is interpreted to comprise
283 small stacked and amalgamated microbial carbonate mounds forming a complex mound

284 system (Somerville et al. 1996; Fernández et al. 2006; Rodríguez-Martínez et al. 2012).
285 These mounds, which are only locally interrupted by capping beds in the upper part of
286 the buildups (rudstones), when the bioconstructions grew-up into more turbulent water
287 conditions, above the storm wave base. The occurrence of sparse cyanobacteria suggests
288 at least dysphotic conditions (Lees and Miller 1995; Cózar et al. 2019). Due to the
289 relative abundance of bioclasts, a proximal outer platform setting is interpreted for this
290 interval, like similar interpretations of microbial mounds of equivalent age in southern
291 France (Cózar et al. 2019).

292 The interval I2 also contains microbial mounds with common cyanobacteria and
293 *Algospongia*, which suggest at least dysphotic to euphotic conditions on the platform
294 (Lees and Miller 1995). Due to the lowest abundance in bioclasts, as well as the
295 predominance of fenestellids, a facies change to a more distal outer platform setting is
296 suggested, compared with the previous Mikhailovian interval. The occurrence of
297 breccias composed of micropeloidal pebbles is likely the result of currents or storms
298 that reworked the top of the carbonate mounds (Rodríguez-Martínez et al. 2012).

299 In the interval I3 (upper Venevian-Tarussian), environmental conditions are
300 interpreted as rather similar to those at the base of the succession, in a proximal outer
301 platform setting, which rarely reached storm wave-base (especially in the lower part of
302 the interval). Individual mounds are smaller than in the underlying intervals.

303 The interval I4 (upper Tarussian-lower Protvian) shows a change in the platform
304 facies, interpreted as very shallow-water depositional environments above the fair-
305 weather wave-base (FWWB), with common grainstone facies capping the growth of
306 mounds. The green algae are as abundant in the mounds (in situ) as in the grainstone
307 beds (transported). Such abundance of green algae in Mississippian microbial facies is
308 only known in the Montagne Noire of France (Cózar et al. 2018b, 2019). The inferred

309 shallow-water conditions, even with some levels reaching the wave-base, suggest a
310 distal inner platform setting. The common packstone and breccia beds are interpreted as
311 storm-related deposits in a shallow-water setting.

312 The interval I5 (Protvian in age) suggests the microbial mounds developed in an
313 environment of slightly deeper water than in the underlying Tarussian-lower Protvian
314 interval. Although still in rather shallow-water conditions in the proximal outer
315 platform, it was rarely affected by storms. Individual morphology of the mounds is still
316 recognizable.

317 The Zapaltjubian interval I6, is characterized by packstones interpreted as
318 tempestites, but also with common oolitic grainstone beds (incipient bars; Rankey et al.
319 2006), which suggest frequent intertidal conditions. Hence, these sediments were
320 probably deposited in a distal setting of the inner platform. The microbial boundstones
321 did not form domical shapes but instead, occur as stratiform layers among the bioclastic
322 beds (interval I6 in Fig. 4c).

323 The interval I7 (Zapaltjubian-Voznesenian) shows marked lithologic differences
324 compared to the underlying intervals. Here the carbonates seem to have accumulated in
325 low energy protected areas, between the fair-weather storm-base (FWSB) and the
326 FWWB, somewhat similar to lagoons, although the location of a fringing margin of the
327 platform is unknown. A possibility is that the previous microbial mounds developed
328 palaeorelief allowing areas of protections from storm and tidal currents, but not
329 generating true restricted lagoons, because the high diversity of bioclasts indicates
330 unrestricted water circulation. Similarly protected areas behind Mississippian microbial
331 mounds and bioclastic shoals are known in basins from southwest Spain (Cózar et al.
332 2006), as well as in other time periods (e.g., Read 1985; Blomeier and Reijmer 1999;
333 Tucker 2003; Flügel 2004; Bosence 2005). However, this low-energy environment was

334 occasionally influenced by storm episodes, characterized by packstone facies, and
335 locally oolitic bars occur in the Cheese Cave area. The occurrence of mud cracks and
336 pedotubules suggest subaerial exposure of the upper part of the succession, indicating a
337 shallowing trend and emersion of the platform, although the absence of well-developed
338 palaeosols could be due to non-preservation caused by post-Bashkirian erosion.

339

340 **Las Llamas-Bejes and La Hermida subunits**

341 These successions are exemplified by the Pompedrei Bridge section (in Las Llamas-
342 Bejes subunit; Fig. 5). The carbonates assigned to the Protvian (Serpukhovian) are
343 predominantly packstones (Facies F11 in Table 1; Fig. 5a), and rarely bioclastic
344 grainstones and mudstones (Facies F7, F13). Packstones and grainstones are usually
345 medium- to coarse-grained, showing moderate to good sorting, and a high degree of
346 packing. Parallel and cross-laminations are recognized. Fining-upward sequences, as
347 well as coarsening-upward sequences occur rarely (Fig. 5b). The bioclasts are highly
348 fragmented, with the main bioclasts being crinoid, bryozoans and brachiopods.
349 *Praedonezella* fragments and micritic lithoclasts are relatively common. Grainstones
350 show similar bioclasts and a higher abundance of calcispheres. Interbedded mudstones
351 mostly contain ostracods and crinoid fragments.

352 The overlying Millaró Member (youngest member of the Alba Formation; Fig. 2a)
353 is more bioclastic than the nodular limestones and shales with ostracods and
354 cephalopods typically described from the CZ. The member is composed of mudstones,
355 packstones and breccias (Facies F7, F11, F16; Fig. 5) interbedded with black siliceous
356 shales and cherts. Limestone facies are predominantly mudstones (Fig. 5c), rarely
357 wackestones, but bioclastic horizons occur. Some beds contain a significant amount of
358 large bioclasts (crinoids, *Calcifolium*, *Praedonezella* and foraminifers in decreasing

359 abundance order), although generally limestones are very fine-grained (Fig. 5d), and
360 also contain typical open marine bioclasts (e.g., radiolarians, ostracods, sponge spicules,
361 thin-shelled molluscs). These bioclastic beds show parallel to wavy lamination with
362 preferred orientation of *Calcifolium* and are well-sorted with a high degree of
363 fragmentation. Rudstones show varied facies ranging from bioclastic wackestone-
364 packstone to mudstone, rarely micropeloidal.

365 A 20 m-thick interval of the Barcaliente Formation is recognized above the Millaró
366 Member. It is mostly composed of organic-rich black mudstones containing ostracods,
367 sponge spicules and radiolarian casts. In addition, there are very thin layers (1–3 cm
368 thick) of pale grey limestone, mostly peloidal to bioclastic cementstone and
369 wackestones (Fig. 5e–f) with parallel lamination, with fining-upwards sequences (Fig.
370 5g). Some rudstone, mudstone-wackestone and microbial facies are recorded in the
371 Pompedrei Bridge section (Facies F6), which probably represents a continuation of the
372 facies recorded in the Millaró Member.

373 The Barcaliente Formation is overlaid by a substantial thickness of clotted facies of
374 the Valdediezma Limestone deposited during the uppermost Zapaltjubian and the
375 Voznesenian (about 350–400 m in the Sierra de Bejes). Textures are mostly
376 cementstones and cement-supported micropeloidal facies (Fig. 5h), interbedded with
377 rare mudstones. Thick and massive bedding dominates and dome-shape mounds were
378 not observed in the field. The younger part of the succession is characterized by more
379 bioclastic clotted limestones, locally developed as non-microbial packstones and
380 wackestones.

381

382 *Interpretation.*— The basal grainstone and packstone deposits developed during the
383 Protvian, are interpreted as turbidites, whereas the rare interbedded mudstones formed
384 the background slope sedimentation (e.g., Reijmer et al. 2012, 2015; Cózar et al. 2017).

385 In the Millaró Member (described as a condensed pelagic limestone-shale interval
386 in the Cantabrian Zone according to Sanz-López et al. 2004, 2007), the carbonates
387 recorded in the Pompedrei Bridge section are interpreted as turbidites (wackestone and
388 packstones) with background slope sedimentation of mudstones and shales. Rudstones
389 are considered distal debris flows due to the small size of the clasts (Flüegel 2004;
390 Payros and Pujalte 2008; Reijmer et al. 2015). The very distal turbidite sedimentation
391 with more frequent open marine fauna (Reijmer and Everaars, 1991), and the
392 siliciclastic component in the black shales, suggest a distal slope or toe-of-slope
393 environment for the Millaró Member.

394 A predominance of suspension background sedimentation in a quiet and restricted
395 basin is inferred for the Barcaliente Formation, which was interrupted by very distal
396 turbidites in the CZ (Evers 1967; Hemleben and Reuther 1980). Some authors have
397 suggested restricted circulation and a degree of temporal anoxia on the sea-bottom,
398 based on the laminated limestones, presence of organic matter, and scarce fossil content
399 (Reuther 1977; Sanz-López et al. 2013). Well-oxygenated sea bottom periods must have
400 alternated with poorly oxygenated conditions because bioturbation is present (Hemleben
401 and Reuther 1980). A moderate water depth in the outer continental shelf has been
402 inferred from bioturbation fabrics (Reuther 1977), with common ichnofossils
403 *Scalarituba*, *Muensteria*, rare *Phycosiphon*, *Gyrophylles*, *Neonereites* and the absence
404 of meandering forms, and burrows of suspension feeders.

405 The overlying Valdediezma Limestone represents a marked change from the deep-
406 water settings of the Barcaliente Formation. Boundstones of microbially-mediated

407 facies are prevalent, although mound morphologies are not recognized. These
408 boundstones contain poorly represented bioclastic facies and seem rather different from
409 the microbial mounds observed in the platform facies of the Saigu subunit. This poverty
410 of bioclasts is interpreted to characterize the deepest part of the outer platform, or
411 possibly the uppermost slope (Cózar et al. 2019). In the upper part of the section,
412 capping beds are present, as well as the slightly richer bioclastic content, which are
413 more typically developed on distal outer platform settings.

414 A similar succession of microbial and bioclastic-microbial limestones, but cut by
415 faults, occurs in the path from the Jitu l'Escarandi to the Casetón de Andara section in
416 the western part of the same tectonic subunit (Fig. 2b).

417

418 **Mesa Sin Pan subunit**

419 The Tournaisian to upper Viséan part of the Mesa Sin Pan section shows a reduced
420 thickness compared to other parts of the succession and a lower abundance of skeletal
421 grains (Fig. 6a). At the base occurs two metres of reddish mudstone to wackestone with
422 bryozoans and echinoderm fragments, partly as coated grains enriched in ferrous oxides
423 (Facies F12 in Table 1). Conodonts indicate the upper Tournaisian *Scaliognathus*
424 *anchoralis* Zone with *Gnathodus mirousei*, *G. pseudosemiglaber* and *Vogelgnathus*
425 *simplicatus*. Above are about 45 m of mudstones and wackestones (Facies F7–F9),
426 breccias and micritic-peloidal cement- supported and matrix-supported beds (Facies F2-
427 F4). Laminated dark grey to black mudstones with radiolarians represent intervals of
428 quiet and deep-water sedimentation. Grey-coloured skeletal wackestones and
429 packstones show fining-upward sequences and parallel lamination. Rudstone beds
430 consist of micropeloidal pebbles and locally show reddish colour associated with
431 stylolites.

432 Above is an upper Serpukhovian interval composed of limestone with black shales
433 and cherts, suggesting a correlation with the Millaró Member of the other tectonic units.
434 Carbonates in this interval are composed of mudstone to bioclastic packstone beds (see
435 facies in Table 1).

436 Higher up in the succession, a 100 m-thick interval of Zapultjubian age consists of
437 cementstones and micropeloidal textures, with low bioclastic content, dominated by
438 *Praedonezella*, fenestellid bryozoans and crinoids. It corresponds to thick-and massive
439 bedded limestones with rare rudstone beds.

440 In the upper part of the succession, the Barcaliente Formation is more than 150 m
441 thick below the Triassic. Lowermost Bashkirian conodonts occur about 130 m above the
442 base of the formation (sample MSP-5 in Fig. 6).

443

444 *Interpretation.*— The abundance of beds with skeletal and reworked grains and rare
445 microbial mudstone occurrences (interpreted as small mounds) suggest a toe-of-slope
446 setting for the lower part of the succession.

447 The upper Serpukhovian mudstone to packstone beds were deposited as turbidites
448 on the slope and the toe-of-slope, where micrite represents the background
449 sedimentation, similar to the better-preserved beds of the Millaró Member in other
450 sections.

451 The second interval of the Valdediezma Limestone (Zapaltjubian age) contains
452 textures and bioclasts which suggest microbial mounds in deep-water conditions,
453 similar to those in the upper part of the Pompedrei Bridge section.

454 The overlying Barcaliente Formation contains only scarce and distal turbidite beds
455 in a prevailing quiet and deep-water environment.

456

457 **Varera subunit and ACVS thrust sheet**

458 The Varera tectonic subunit (Fig. 2b) includes a slice of basal Cambrian rocks below the
459 Alba Formation and the Valdediezma Limestone (Argaña section, Fig. 6b). The Alba
460 Formation occurs below the Valdediezma Limestone in the ACVS (southwards of the
461 Tejo unit). It consists of ammonoid-bearing nodular pink to reddish to grey limestone.
462 The nodular to well-stratified lime mudstone to wackestones commonly display
463 bioturbation, ferromanganese crusts over the intraclasts and bioclasts, as well as
464 hardground surfaces. Fossil content is concentrated in bioclastic bands and includes
465 sponge spicules, ostracods, conodonts, radiolarians, ammonoids and more rarely
466 crinoids, molluscs, bryozoans, brachiopods and trilobites. Bioclastic limestones are
467 abundant in the upper five meters of the Canalón Member in the Cueto de los Senderos
468 and Vegas de Sotres sections (Figs. 6c, 7). These beds are commonly 2 to 5 cm thick,
469 and interbedded with mudstone-wackestone to packstones. Elongated bioclasts show a
470 slight preferred orientation and locally cross-lamination to wavy-lamination occur.
471 Those beds do not differ significantly from the overlying Valdediezma Limestone,
472 except for the prevailing pinkish colour of the nodular limestone.

473 Higher up, the well-bedded Valdediezma Limestone consists predominantly of
474 packstones to wackestones, in beds that are 5 to 20 cm, rarely up to 50 cm thick, often
475 with irregular bases and tops (lithological unit 2 in Figs. 6–7). Rarely, thin pale grey
476 nodular beds are interbedded. Shale partings of millimeter thickness occur rarely. The
477 main feature of the Valdediezma Limestone is the high bioclastic content, with a
478 relative mixture of typical deep-water fossils (sponge spicules, radiolarians) and more
479 typical shallow-water organisms (abundant foraminifers, abundant calcispheres,
480 *Kamaenella*, brachiopods). The bioclasts are always fine- to very fine-grained, although
481 the amount of micrite matrix varies significantly, resulting in a range of mudstone to

482 packstone textures (locally grainstones; Facies F12; Fig. 7c–g). Fining-upward cycles
483 occur, but coarsening-upward cycles are more common (less than 1 cm thick, and up to
484 4–5 cm thick). The mudstones contain sponge spicules and ostracods like those in the
485 Canalón Member (reddish to pink), but with a different colour (pale grey).

486 The overlying dark grey limestone (lithological unit 3 in Figs. 6–7) consists of
487 intraclastic-bioclastic mudstones to rudstones (Fig. 7h), with chert nodules. Packstone
488 levels show grading. Angular intraclasts are commonly observed within the mudstone
489 and wackestone textures and, rounded grainstone intraclasts occur rarely. Pebbles
490 include bioclastic packstones and grainstones from shallow-water settings (common
491 algaespongiids, foraminifers, bryozoans, ostracods, molluscs, as well as rare conodonts,
492 sponge spicules, trilobites and red algae), including silicified macrofossils (solitary and
493 branching rugose corals, brachiopods and crinoids). The diverse foraminiferal
494 assemblages recognized in this unit, with typical taxa of the shallow-water platform is a
495 noteworthy feature (see full list of taxa in Cózar et al. 2016, 2018a).

496

497 *Interpretation.*— The typical griotte nodular limestones exposed at the base of the
498 sections have been interpreted as deep-water and condensed sediments that were
499 deposited at a depth of some hundreds of metres (Tucker 1974; Wendt and Aigner
500 1985). The bioclastic horizons mostly recorded in the uppermost part of the Alba
501 Formation are interpreted as distal turbidites.

502 Bioclastic beds of the Valdediezma Limestone are mostly interpreted as turbidites
503 deposited in a hemipelagic setting that transported material from the outer part of a
504 shallow-water platform into the basin. This inference is based on the predominant
505 foraminiferal genera recorded in the resedimented material, such as the lasiodiscids,
506 suggesting a calm environment in the outer platform and highly tolerant genera (such as

507 the archaedisks, *Mediocris* and *Tetrataxis*, according to Cózar and Rodríguez 2003).
508 The inverse grading observed in numerous beds, may represent typical turbidites
509 alternating with turbidites reworked by deep-water bottom currents (e.g. Stanley 1988;
510 Rebesco et al. 2014; Shanmugam 2017), suggestive of a distal slope setting, inferred
511 from the size as well as the occurrence of reworking (i.e. contour currents).

512 The deposition of unit 3 corresponds to a lower slope setting with debris-flow
513 deposits within the turbidite system. Grainstone intraclasts and its fossil content suggest
514 transportation from shallow-water platform facies, whereas intraclasts of mudstone to
515 wackestone seem to have been derived from microbial mounds developed in the upper
516 slope or from early cemented beds on a stepped slope.

517

518 **Discussion**

519

520 **Reconstruction of the Valdediezma platform**

521 The environments of the Valdediezma platform are reconstructed based on stratigraphic
522 profiles from a northwest to southeast transect across the different tectonic subunits
523 (Figs. 2b, 8). Outer (below the FWSB) to distal inner (above the FWSB and commonly
524 affected by the FWWB) platform facies are preserved in the Saigu subunit, outer
525 platform to slope facies are in the Las Llamas-Bejes and La Hermida subunits, and toe-
526 of-slope and basin facies occurs interbedded in the Las Llamas-Bejes subunit (Millaró
527 Member and Barcaliente Formation). The lower slope to toe-of-slope and basin settings
528 are interpreted for the Mesa Sin Pan section, where the Barcaliente Formation partly
529 interdigitates with the upper part of the Valdediezma Limestone. Although the thrust
530 sheets do not allow continuous lateral facies changes to be recognised, the correlation of
531 the sections suggests a platform margin with an approximate southwest to northeast

532 trend (current geographic coordinates). The transition from the platform into the basin
533 in the southwest is apparently more abrupt compared to that in the southeast, because
534 below the Saigu subunit, the Varera subunit consists of several slices with different
535 stratigraphy and important fault movements related to the San Carlos Fault. The
536 northern margin of the Valdediezma platform is buried below the Gamonedo-Cabrales
537 thrust sheet, and Mesozoic rock cover in its eastward continuation. The shallow-water
538 platform in the Tejo unit extends for some 5 by 28 kilometres. According to the
539 reconstruction of the open Asturian Arc by Pastor-Galan et al. (2011), the original
540 orientation of the core of the Picos de Europa province remained unaltered, and thus, the
541 original orientation of the Valdediezma platform was similar to the current orientation.

542 Shallow-water sedimentation was initiated in the upper Tournaisian based on the
543 conodont evidence indicating the oldest transported sediments in the Mesa Sin Pan
544 subunit (Fig. 8). There, lower to upper Viséan carbonate breccias are at the toe-of-slope,
545 together with thin microbial boundstone beds. High carbonate production rates during
546 the upper Viséan to lower Serpukhovian (associated with the higher sedimentation rate
547 of microbial mounds), are recognized in the carbonate platform facies of the Saigu
548 subunit (Fig. 8). The microbial mound growth occurred from the outer platform to the
549 upper slope. Boundstones of several metres palaeoheight and similar width occurred on
550 the shallow-water platform, whereas thick and massive-bedded limestones are observed
551 in the outer part of the platform. The thickness and facies of the Valdediezma
552 Limestone in the Saigu and the Las Llamas-Bejes subunits (about 520 m) contrast
553 markedly with the thinness of the condensed sections in the southern toe-of-slope and
554 basinal facies (from 10 to 60 metres). These abrupt changes in the Mississippian
555 successions suggest a steep margin for the platform (Fig. 8), possibly induced by the
556 rapid growth of the microbial boundstones. The rapid sedimentation rate of microbial

557 mounds is a common feature in the younger Pennsylvanian carbonate platform of the
558 CZ and in other platforms known from the geological record, causing high-relief
559 carbonate platforms with step margins (e.g., Bechstädt et al. 1985; Neuweiler 1993;
560 Kenter et al. 2005; Bahamonde et al. 2007; Olivier et al. 2011).

561 Calciturbidites with bioclasts that were derived from the shallow-water platform
562 formed a lateral wedge, which extended to the southern part of the basin. Progradation
563 of this wedge is recognized from the upper Viséan (Venevian) based on the evidence of
564 interbedded units within the Canalón Member of the eastern part of the ACVS. An
565 increase in the amount of transported sediments is recognised from the lower to the
566 upper Serpukhovian (Tarussian to Protvian). The lateral wedge thins along the toe-of-
567 slope, from a maximum of ca. 140 m in the Argaña, Pompedrei Bridge and Mesa Sin
568 Pan sections (Tejo unit) to less than 10 m at the Vegas de Sotres section in the south
569 (ACVS; Fig. 8). Protvian bioclastic and intraclastic limestones occur in the outer
570 platform to slope transition (Las Llamas-Bejes and La Hermida subunits). Debris flows
571 are scarce but breccias occur in the Protvian of unit 3 at the Vegas de Sotres section.
572 These facts, together with the different thicknesses between the shallow-water and the
573 basinal carbonates, suggest a steep-fronted platform margin

574 The disappearance of calciturbidites during the upper Serpukhovian in the ACVS
575 coincides with the Millaró Member or a thick interval (20 m thick) in the southern
576 margin of the Valdediezma Limestone (Las Llamas-Bejes and Mesa Sin Pan subunits;
577 Fig. 8). This member was deposited during an extended drowning episode at the top of
578 the Alba Formation in the CZ. It was described as a condensed, pelagic deep-water
579 limestone-shale interval with abundant benthonic and nektonic faunas by Sanz-López et
580 al. (2004, 2007). The Millaró Member includes thin distal deposits with platform-

581 derived bioclasts in the Tejo unit and its occurrence there suggests back-stepping of the
582 platform area with high carbonate production (Fig. 8).

583 The microbial and skeletal carbonate factory fed sediments to the area of the
584 southern slope of the Valdediezma platform, starting in the upper Serpukhovian
585 (Zapaltjubian in Fig. 8; Las Llamas-Bejes, La Hermida and Mesa Sin Pan subunits).
586 This shallow-water interval is absent in the Barcaliente Formation of the ACVS.
587 Thicknesses (and accumulation rates) are similar for the upper part of the Valdediezma
588 Limestone and the Barcaliente Formation, contrasting with divergent thicknesses of the
589 Alba Formation and the lower part of the Valdediezma Limestone (Fig. 8). This similar
590 thickness in carbonates of the upper Valdediezma Limestone and the Barcaliente
591 Formation coincides with the upper Serpukhovian, high rate of subsidence and
592 deepening trend of the foreland system of the CZ (Sanz-López et al. 2013).

593 The latest Serpukhovian-early Bashkirian deep-water carbonate sedimentation of
594 the Barcaliente Formation extended from the foreland margin into the foredeep (filled
595 by siliciclastic turbidites) in the westernmost CZ (Sanz-López et al. 2006). It coincides
596 with the deposition of the Barcaliente Formation on the southern margin of the
597 Valdediezma platform (Las Llamas and Mesa Sin Pan subunits in Fig. 8). The
598 Barcaliente Formation shows high accumulation rates in a moderately deep basin with
599 carbonate sediment re-distributed by currents. The accumulation rate on the platform
600 and the basin were similar and subsidence rates are likely similar between both areas.
601 (Fig. 8). The shallow-carbonate platform showed continued growth during
602 sedimentation of the Barcaliente Formation into the early Bashkirian (Krasnopolyanian,
603 Kinderscoutian). Microbial boundstones and skeletal limestones occurred in the outer
604 platform to slope (Las Llamas-Bejes subunit), whereas microbial mounds and bioclastic
605 shoals sheltered low-energy areas on the inner platform (Saigu subunit).

606 The Valdediezma platform is interpreted as an isolated shallow-water platform (in
607 the sense of Read 1985), or an unattached platform or major offshore bank in the sense
608 of Bosence (2005). This platform developed in a starved basin with prevailing pelagic
609 sedimentation of cephalopod-bearing nodular limestone (Alba Formation) in the
610 western margin of Palaeotethys Ocean during the upper Tournaisian-Serpukhovian
611 (Sanz-López et al. 2018). In the western part of the Palaeotethys Ocean, this contributed
612 to shallow-water carbonate ramp also known from the late Tournaisian of the Montagne
613 Noire (South France) to the late Serpukhovian (Protvian), although mainly known from
614 olistoliths and klippe (Vachard et al. 2017; Cózar et al. 2017, 2019). Microbial mound
615 development on these carbonate ramps and siliciclastic platforms was contemporaneous
616 with deep-sea fan sedimentation in the Montagne Noire basin from the late Viséan
617 (Mikhailovian age). This age interval corresponds to the high carbonate production
618 observed in the Valdediezma platform, which persisted from the latest Serpukhovian to
619 the early Bashkirian, when Variscan deformation had exhumed the Montagne Noire
620 ramp. This tectonic event may relate to the late Serpukhovian deepening trend of the
621 Millaró Member in the CZ. The previous Serpukhovian progradational wedge
622 associated with the accumulation of microbial boundstone of the Valdediezma platform,
623 also coincides in time with the Serpukhovian progradational wedge described by Collins
624 et al. (2006) in the Tengiz build-up in the subsurface of the Precaspian Basin
625 (Kazakhstan) also part of the Palaeotethys Ocean. Relationships of the Valdediezma
626 progradational wedge with Variscan tectonics and/or eustasy are yet to be analyzed.

627

628 **Nucleation of the platform**

629 The substrate of the Valdediezma Limestone seems to be the Cambrian rocks that are
630 tectonically detached in the Varera subunit. Erosion of the sedimentary sequence down

631 into middle Cambrian rocks is the deepest known below the uppermost Devonian-
632 Mississippian unconformity of the CZ. This erosion was previously inferred to be
633 related to the westwards tilt of the passive margin and denudation of the peripheral
634 bulge in the foreland basin (Martínez García 1978; Keller et al. 2007). An alternative is
635 that the initial growth of the Valdediezma platform may have started on a submarine
636 topographic high that induced carbonate sediment accumulation in the Tejo unit. The
637 Picos de Europa Province (where the Valdediezma platform developed) has been
638 recognized as a block displaying submarine relief during the Mississippian (Eichmüller
639 and Seibert 1984). Basin segmentation into uplifted blocks and troughs bounded by
640 extensional faults was interpreted on the basis of facies distributions, the occurrence of
641 breccias, debris flows and slump deposits in the Alba Formation, although actual faults
642 responsible were not identified (Wendt and Aigner 1985). Distribution of chert and
643 shale sedimentation (of the Lavandera Member) associated with troughs, suggests
644 location of submarine relief in areas with carbonate sedimentation (Fig. 9). Thus, the
645 Valdediezma Limestone seems to correspond to an isolated platform developed on a
646 horst structure (e.g. Blomeier and Reijmer 1999). Sedimentary highs and basins
647 (probably horst and graben topography) have been similarly interpreted from
648 Mississippian pelagic carbonate deposits of southern Europe, from the Pyrenees,
649 Catalonian Coastal Ranges and the Southern Alps (Schönlaub and Histon 2000; Sanz-
650 López et al. 2000, Sanz-López 2002; Casas et al. 2019).

651

652 **Demise of the platform**

653 Hemleben and Reuther (1980) proposed a shallowing trend in the upper part of the
654 Barcaliente Formation, ending in an interval with channel development, in situ
655 brecciation, laminations interpreted as stromatolite colonization of the sea bottom, and

656 pseudomorphs of evaporitic crystals (see also Reuther 1977; González Lastra 1978).
657 This shallowing trend spans the uppermost Serpukhovian-lower Bashkirian interval
658 according to Sanz-López et al. (2013), where carbonate accumulation compensates for
659 the basin subsidence, promoting expansion of carbonate sedimentation over the
660 siliciclastic turbidites previously deposited into the foredeep. The occurrence of
661 evaporites and stromatolites suggests high salinity conditions during an early Bashkirian
662 event, but not necessarily a littoral intertidal zone. Both could have occurred in the
663 deep-sea-water restricted basin of the Barcaliente Formation and was clearly
664 differentiated from the contemporaneous shallow-water Valdediezma platform. The
665 shallowing trend in the Barcaliente Formation ended with the occurrence of an
666 intraformational breccia (Porma Breccia) in most areas of the CZ. Shallowing events in
667 the Voznesenian/Krasnopolyanian age interval of the Valdediezma and Barcaliente
668 successions units seems to be associated with the eastward migration of the foredeep
669 basin depocenter in the CZ. Strong flexure of the active foreland was caused by nearby
670 thrust loading and subsequent filling of the foredeep by Bashkirian to early Moscovian
671 deltaic systems (Marcos and Pulgar 1982); to be followed, by the carbonate platforms of
672 the Valdeteja Formation developed on the adjacent foreland margin (Eichmüller 1985;
673 Bahamonde et al. 2015; Chesnel et al. 2016). The strong flexure of the active foreland
674 and the migration of the forebulge area eastwards, also caused the exhumation of the
675 Valdediezma platform at the distal craton edge, based on the non-deposition (or erosion)
676 of the lower Bashkirian to Moscovian strata. Flexure of the foreland would have
677 generated significant seafloor relief differences between the Valdediezma platform
678 (several hundreds of metres thick) and the basinal carbonates (where the Alba
679 Formation is ca. 10 metres thick, Fig. 10).

680 Although sedimentation of the Valdediezma Limestone stopped in the early
681 Bashkirian, Pennsylvanian microbial boundstone-dominated carbonates accumulated in
682 the basin adjacent to the Valdediezma platform due to the relief on the palaeo-seafloor.
683 The Bashkirian-Moscovian platforms accumulated some 720 m of thickness and
684 covered more than 12,000 km² according to Bahamonde et al. (2007). These authors
685 differentiated a Bashkirian carbonate ramp (Valdeteja Formation) which evolved to a
686 Moscovian-lower Kasimovian flat-topped carbonate platform with steep margins (Picos
687 de Europa Formation). The inner facies of both platforms were located in the Tejo unit
688 where the older Valdediezma platform is now recognized (Fig. 10).

689 The burial of the Valdediezma Limestone by the uppermost part of the Picos de
690 Europa Formation corresponds to the tectonic subsidence of the Picos de Europa
691 Province starting from the late Myachkovian (latest Moscovian). According to Merino-
692 Tomé et al. (2009) this subsidence was related to the thrusting and southwards
693 emplacement of the Ponga Nappe Province (Figs. 2b, 10).

694

695 **Conclusions**

696

697 The Valdediezma Limestone was deposited on an isolated platform located in the distal
698 margin of the Carboniferous Variscan foreland (Picos de Europa province). The onset of
699 this carbonate platform started during the upper Tournaisian on a topographic high
700 differentiated from the deep-water sedimentation of griotte limestone in the starved
701 basin. The oldest skeletal and lithoclastic sediments with rare microbial limestones crop
702 out only locally. A high subsidence rate balanced by high carbonate production in
703 shallow-water settings resulted in the accumulation of some 800 m of platform
704 succession from the upper Viséan to the lower Bashkirian. Differences in the

705 accumulation of carbonates in the platform and the basin, and the studied slope facies,
706 suggest the Mississippian high-relief platform formed prior to the well-documented
707 Pennsylvanian platforms in the CZ. Sediments derived from the shallow-water platform
708 extended southwards as a thin lateral wedge that accumulated at the toe-of-slope and
709 basin from the upper Viséan but mainly during the Serpukhovian. The progradation of
710 this wedge ended in the upper Serpukhovian when drowning was recorded on the
711 platform margin. This drowning coincided with a regional, deepening event in the CZ
712 (coeval with the Millaró Member), which increased the faunal abundance in the deep
713 basin. Higher subsidence and sedimentation rates in the foreland were associated with
714 the migration of the foredeep at the western margin of the CZ and the supply of
715 synorogenic siliciclastics supplied from the active orogenic front. The moderately deep-
716 water carbonate sedimentation of the Barcaliente Formation was restricted to the
717 foreland margin where occasionally restricted bottom circulation favoured a stratified
718 water column, whereas nearby high productivity was maintained in the water surface.
719 At this time, the shallow-water carbonate material derived from the Valdediezma
720 platform was deposited on its southern margin. Between the uppermost Serpukhovian
721 and the early Bashkirian, the Valdediezma platform retreated, and finally during the
722 Voznesenian-Krasnopolyanian, a shallowing trend is seen that coincides with that
723 recognized in the basinal Barcaliente Formation. The demise of the Valdediezma
724 platform was caused by its uplift during the migration of the successive foredeep
725 depocenters, and flexure of the forebulge, generating seafloor topographic relief.
726 Pennsylvanian carbonate platforms attached to this relief, which subsequently collapsed
727 and were buried by upper Moscovian shallow-water carbonates.

728

729 **References**

730

731 Baccelle L, Bosellini A (1965) Diagrammi per la stima visiva della composizione
732 percentuale nelle rocce sedimentarie. *Ann Univ Ferrara, Sez IX, Sc Geol e*
733 *Paleontol* 1:59–62

734 Bahamonde JR, Colmenero JR, Vera C (1997) Growth and demise of late
735 Carboniferous carbonate platforms in the eastern Cantabrian Zone, Asturias,
736 northwestern Spain. *Sed Geol* 110: 99–122.

737 Bahamonde JR, Merino-Tomé OA, Heredia N (2007) Pennsylvanian microbial
738 boundstone-dominated carbonate shelf developed in a distal foreland margin (Picos
739 de Europa Province, NW Spain). *Sed Geol* 198:167–193. DOI:
740 10.1016/j.sedgeo.2006.12.004

741 Bahamonde JR, Kenter JAM, Della Porta G, van Hoeflaken F (2008) Facies belts of a
742 Carboniferous carbonate platform (San Antolín-La Huelga section, NE Cantabrian
743 Zone, Northern Spain). *Trab Geol, Univ Oviedo* 28:69–86.

744 Bahamonde JR, Merino-Tomé OA, Della Porta G, Villa E (2015) Pennsylvanian
745 carbonate platforms adjacent to deltaic systems in an active marine foreland basin
746 (Escalada Fm, Cantabrian Zone, NW Spain). *Basin Res* 27: 208–229. DOI:
747 10.1111/bre.12068

748 Bahamonde JR, Della Porta G, Merino-Tomé OA, Villa E (2017) Lateral variability of
749 shallow-water facies and high-frequency cycles in foreland basin carbonate
750 platforms (Pennsylvanian, NW Spain). *Facies* 63, 6. DOI: 10.1007/s10347-016-
751 0487-3

752 Bechstädt T, Boni M, Selg M (1985) The Lower Cambrian of SW-Sardinia: From a
753 clastic tidal shelf to an isolated carbonate platform. *Facies* 12, 113–140. DOI:
754 10.1007/BF02536978

755 Blanco-Ferrera S, Sanz-López J, Cózar P (2017) Mississippian to early Bashkirian
756 conodonts from an exposed shallow-water carbonate platform in the Picos de
757 Europa Unit, Spain. In: Liao J-Ch, Valenzuela-Ríos JI (eds), Fourth International
758 Conodont Symposium. ICOS IV. "Progress on Conodont Investigation". Cuadernos
759 del Museo Geominero 22. Instituto Geológico y Minero de España, Madrid, pp
760 215–218.

761 Blomeier DPG Reijmer JGG (1999) Drowning of a Lower Jurassic Carbonate Platform:
762 Jbel Bou Dahar, High Atlas, Morocco. *Facies* 41:81–110. Bosence D (2005) A
763 genetic classification of carbonate platforms based on their basinal and tectonic
764 settings in the Cenozoic. *Sed Geol* 175:49–72. DOI: 10.1016/j.sedgeo.2004.12.03

765 Bosence D (2005) A genetic classification of carbonate platforms based on their basinal
766 and tectonic settings in the Cenozoic. *Sed Geol* 175:49–72. DOI:
767 10.1016/j.sedgeo.2004.12.030

768 Casas JM, Álvaro JJ, Clausen S, Padel M, Puddu C, Sanz-López J, Sánchez-García T,
769 Navidad M, Castiñeiras P, Liesa M (2019) Palaeozoic basement of the Pyrenees. In:
770 Quesada C, Oliveira J (eds), *The geology of Iberia: a geodynamic approach*,
771 volume 2: The Variscan Cycle. Springer, Cham, pp. 229–259.

772 Chesnel V, Samankassou E, Merino-Tomé OA, Fernández LP, Villa E (2016) Facies,
773 geometry and growth phases of the Valdorria carbonate platform (Pennsylvanian,
774 northern Spain). *Sedimentology* 63:60–104. DOI: 10.1111/sed.12221

775 Collins JF, Kenter JAM Harris PM, Kuanysheva G, Fischer GDJ, Steffen KL (2006)
776 Facies and reservoir-quality variations in the late Viséan to Bashkirian outer
777 platform, rim, and flank of the Tengiz buildup, Precaspian Basin, Kazakhstan. In:
778 Harris PM, Weber LJ (eds), *Giant hydrocarbon reservoirs of the world: From rocks*

779 to reservoir characterization and modelling. AAPG Mem 88/SEPM Spec Publ,
780 Tulsa, pp. 55–95. DOI:10.1306/1215874M881469

781 Colmenero JR, Fernández LP, Moreno C, Bahamonde JR, Barba P, Heredia N,
782 González F (2002) Carboniferous. In: Gibbons W, Moreno MT (eds), The Geology
783 of Spain. Geological Society, London, pp. 93–116.

784 Corrochano D, Barba P, Colmenero JR (2012a) Glacioeustatic cyclicality of a
785 Pennsylvanian carbonate platform in a foreland basin setting: an example from the
786 Bachende Formation of the Cantabrian Zone (NW Spain). Sed Geol 245–246:76–
787 93. DOI: 10.1016/j.sedgeo.2011.12.009

788 Corrochano D, Barba P, Colmenero JR (2012b) Transgressive-regressive sequence
789 stratigraphy of Pennsylvanian *Donezella* bioherms in a foreland basin (Lena Group,
790 Cantabrian Zone, NW Spain). Facies 58:457–476. DOI: 10.1007/s10347-011-0282-
791 0

792 Cózar P, Rodríguez S (2003) The palaeoecological distribution of the endothyroids
793 (Foraminifera) in the Guadiato area (SW Spain, Mississippian). Palaeogeogr
794 Palaeoclimatol Palaeoecol 201:1–19. DOI: 10.1016/S0031-0182(03)00459-0

795 Cózar P, Somerville ID, Rodríguez S, Mas R, Medina-Varea P (2006) Development of a
796 late Viséan (Mississippian) mixed carbonate/siliciclastic platform in the
797 Guadalmellato Valley (southwestern Spain). Sed Geol 183:269–295. DOI:
798 10.1016/j.sedgeo.2005.09.018

799 Cózar P, Sanz-López J, Blanco-Ferrera S (2015) Late Viséan–Serpukhovian lasiodiscid
800 foraminifers in Vegas de Sotres section (Cantabrian Mountains, NW Spain):
801 potential biostratigraphic markers for the Viséan–Serpukhovian boundary. Geobios
802 48:213–238. DOI: 10.1016/j.geobios.2015.02.006

803 Cózar P, Somerville ID, Sanz-López J, Blanco-Ferrera S (2016) Foraminiferal
804 biostratigraphy across the Viséan/Serpukhovian boundary in the Vegas de Sotres
805 section (Cantabrian Mountains, Spain). *J Foram Res* 46:171–192.

806 Cózar P, Izart A, Vachard D, Coronado I (2017) A mid-Tournaisian-late Viséan
807 carbonate ramp reconstructed from nappes and olistolites in the southern Montagne
808 Noire (France). *Sed Geol* 358:148–175. DOI: 10.1016/j.sedgeo.2017.07.007

809 Cózar P, Somerville ID, Blanco-Ferrera S, Sanz-López J (2018a) Palaeobiogeographical
810 context in the development of shallow-water late Viséan-early Bashkirian benthic
811 foraminifers and calcareous algae in the Cantabrian Mountains (Spain).
812 *Palaeogeogr Palaeoclimatol Palaeoecol* 551:620–638. DOI:
813 10.1016/j.palaeo.2018.09.031

814 Cózar P, Somerville ID, Coronado I, Vachard D, Izart A, Aretz M (2018b) States of
815 preservation and role of dasyclad algal mounds in Mississippian carbonate mounds.
816 *Palaios* 33:419–430. DOI: 10.2110/palo.2018.009

817 Cózar P, Izart A, Somerville ID, Aretz M, Coronado I, Vachard D (2019)
818 Environmental controls on the development of Mississippian microbial carbonate
819 mounds and platform limestones in southern Montagne Noire (France).
820 *Sedimentology* 66:2392–2424. DOI: 10.1111/sed.12594

821 Davydov VI, Korn D, Schmitz MD, Gradstein FM, Hammer O (2012) Chapter 23 – the
822 Carboniferous period. In: Gradstein FM, Ogg JG, Schmitz MD, Ogg GM (eds), *The*
823 *Geologic Time Scale 2012*. Elsevier, Amsterdam, pp. 603–651.

824 Della Porta G, Kenter JAM, Immenhauser A, Bahamonde JR (2002) Lithofacies
825 character and architecture across a Pennsylvanian inner-platform transect (Sierra de
826 Cuera, Asturias, Spain). *J Sed Res* 72:898–916.

- 827 Della Porta G, Kenter JAM, Bahamonde JR (2004) Depositional facies and stratal
828 geometry of an Upper Carboniferous prograding and aggrading high-relief
829 carbonate platform (Cantabrian Mountains, NW Spain). *Sedimentology* 51:267–
830 295. DOI: 10.1046/j.1365-3091.2003.00621.x
- 831 Dunham RJ (1962) Classification of carbonate rocks according to depositional texture.
832 In: Ham W.E. (Ed), *Classification of Carbonate Rocks*. AAPG, Mem 1, 108–121.
- 833 Eichmüller K (1985) The Valdeteja Formation: Environment and History of an Upper
834 Carboniferous Platform (Cantabrian Mountains, Northern Spain). *Facies* 13:45–
835 153.
- 836 Eichmüller K, Seibert P (1984) Faziesentwicklung zwischen Tournai und Westfal D in
837 Kantabischen Gebirge (N. W. Spanien). *Z Dtsch Geol Ges* 135:163–191.
- 838 Embry AF, Klovan JE (1971) A Late Devonian reef tract on Northeastern Banks Island,
839 NWT. *Bull Can Pet Geol* 19:730–781.
- 840 Engel W, Feist R, Franke W (1981) Le Carbonifère anté-stéphanien de la Montagne
841 Noire: rapports entre mise en place des nappes et sédimentation. *Bull BRGM*,
842 section 1, 4:341–389.
- 843 Espina RG (1994) Extensión mesozoica y acortamiento alpino en el borde occidental de
844 la Cuenca Vasco Cantábrica. *Cadernos Lab Xeol Laxe* 19:137–150.
- 845 Evers HJ (1967) Geology of the Leonides between the Bernesga and Porma Rivers,
846 Cantabrian Mountains, NW Spain. *Leid Geol Med* 41:83–151.
- 847 Farias P, Heredia N (1994) Geometría y cinemática de los dúplex de Pambuches
848 (Unidad de Picos de Europa, zona Cantábrica, NO de España). *Rev Soc Geol*
849 *España* 7:113–120.
- 850 Fernández LP, Nose M, Fernández-Martínez E, Médez-Bedia I, Schröder St, Soto, F
851 (2006) Reefal and mud mound facies development in the Lower Devonian La Vid

852 Group at the Colle outcrops (León province, Cantabrian Zone, NW Spain. *Facies*
853 52:307–327. DOI: 10.1007/s10347-005-0042-0

854 Flügel E (2004) *Microfacies of carbonate rocks. Analysis, interpretation and*
855 *application*. Springer Verlag, Berlin, Heidelberg, New York.

856 González Lastra J (1978) *Facies salinas en la Caliza de Montaña (Cordillera*
857 *Cantábrica)*. *Trab Geol* 10:249–265.

858 Hemleben CH, Reuther C-D (1980) *Allodapic limestones of the Barcaliente Formation*
859 *(Namurian A) between Luna and Cea Rivers (Southern Cantabrian Mountains,*
860 *Spain)*. *N Jb Geol Paläont Abh* 159:225–255.

861 Julivert M (1971) *Décollement tectonics in the Hercynian cordillera of northwest Spain.*
862 *Am J Sc* 270:1–29.

863 Julivert M (1978) *Hercynian orogeny and carboniferous paleogeography in NW Spain:*
864 *a model of deformation-sedimentation relationships*. *Z Dtsch Geol Ges* 129:565–
865 592.

866 Keller M, Bahlburg H, Reuther CD, Weh A (2007) *Flexural to broken foreland basin*
867 *evolution as a result of Variscan collisional events in northwestern Spain*. In:
868 *Hatcher RD Jr, Carlson MP, McBride JH, Martínez Catalán JR (eds), 4-D*
869 *framework of continental crust*. *Geol Soc Am* 200, pp. 489–510. DOI:
870 10.1130/2007.1200(25)

871 Kenter JAM, Harris PM, Della Porta G (2005) *Steep microbial boundstone-dominated*
872 *platform margins—examples and implication*. *Sed Geol* 178:5–30.

873 Lees A, Miller J. (1995) *Waulsortian banks*. In: *Monty CLV, Bosence DWJ, Bridges,*
874 *PH, Pratt BR (eds) Carbonate Mud-Mounds: Their Origin and Evolution*. IAS
875 *Spec. Public., 23, Blackwell Science, Oxford, pp. 191–271.*

876 Marcos A, Pulgar JA (1982) An approach to the tectonostratigraphic evolution of the
877 Cantabrian Foreland thrust and fold belt, Hercynian Cordillera of NW Spain. *N Jb*
878 *Geol Paläont Abh* 163:256–260.

879 Marquínez J (1989) Mapa Geológico de la Región del Cuera y Picos de Europa
880 (Cordillera Cantábrica, NW de España). *Trab Geol* 18:137–144.

881 Martínez García E (1978) El Cámbrico de los Picos de Europa. *Trab Geol* 10:341–350.

882 Merino-Tomé OA, Bahamonde JR, Colmenero JR, Heredia N, Villa E, Farias P (2009)
883 Emplacement of the Cuera and Picos de Europa imbricate system at the core of the
884 Iberian-Armorican Arc (Cantabrian Zone, NW Spain). New precisions concerning
885 the timing of arc closure. *Geol Soc Am Bull* 121:729–751. DOI: 10.1130/B26366.1

886 Merino-Tomé OA, Suárez-Rodríguez A, Alonso JL, González-Menéndez L, Heredia N,
887 Marcos-Vallaure A (2014) Mapa Geológico Digital Continuo, E. 1:50.000,
888 Principado de Asturias (Zonas: 1100-1000-1600). In: Navas J (Ed), GEODE. Mapa
889 Geológico Digital Continuo de España. Sistema de Información Geológica
890 Continua: SIGECO. IGME. <http://cuarzo.igme.es/sigeco.default.htm>.

891 Neuweiler F (1993) Development of albian microbialites and microbialite reefs at
892 marginal platform areas of the Vasco-Cantabrian Basin (Soba reef area, Cantabria,
893 N. Spain). *Facies* 29:231–249. DOI: 10.1007/BF02536930

894 Oliveira JT, González Clavijo E, Alonso JL, Armendáriz M, Bahamonde JR, Braid JA,
895 Colmenero JR, Dias Da Silva I, Fernandes P, Fernández LP, Gabaldón V, Jorge
896 RCGS, Machado G, Marcos A, Merino-Tomé O, Moreira N, Murphy JB, Pinto de
897 Jesus A, Quesada C, Rodrigues B, Rosales I, Sanz-López J, Suárez A, Vilam E,
898 Piçarra JM, Pereira Z (2019) Synorogenic Basins. In: Quesada C, Oliveira J (eds),
899 The geology of Iberia: a geodynamic approach, volume 2: The Variscan Cycle.
900 Springer, Cham, pp. 349–429.

901 Olivier N, Colombié C, Pittet B, Lathuilière B (2011) Microbial carbonates and coral on
902 the marginal French Jura platform (Late Oxfordian, Molinges section). *Facies*
903 57:469–492. DOI: 10.1007/s10347-010-0246-9

904 Pastor-Galán, D., Gutiérrez-Alonso, G., Weil, A.B., 2011. Orocline timing through joint
905 analysis: Insights from the Ibero-Armorican Arc. *Tectonophysics* 507:31–46.

906 Payros A, Pujalte V (2008) Calciclastic submarine fans: An integrated overview. *Earth-*
907 *Sc Rev* 86:203–246. DOI: 10.1016/j.earscirev.2007.09.001

908 Pérez- Estaún A, Bastida F, Alonso JL, Marquínez J, Aller J, Álvarez Marrón J, Marcos
909 A, Pulgar J (1988) A thin- skinned tectonics model for an arcuate fold and thrust
910 belt: The Cantabrian Zone. *Tectonics* 7:517–537.

911 Rankey EC, Riegl B, Steffen K (2006) Form, function and feedbacks in a tidally
912 dominated ooid shoal, Bahamas. *Sedimentology* 53:1191–1210. DOI:
913 10.1111/j.1365-3091.2006.00807.x

914 Read JF (1985) Carbonate platform facies models. *AAPG Bull* 69:1– 21.

915 Rebesco M, Hernández-Molina FJ, van Rooij D, Wåhlin A (2014) Contourites and
916 associated sediments controlled by deep-water circulation processes: stage-of-the-
917 art and future considerations. *Mar Geol* 352:111–154. DOI:
918 10.1016/j.margeo.2014.03.011

919 Reijmer JJG, Everaars JSL (1991) Carbonate platform facies reflected in carbonate
920 basin facies (Triassic, Northern Calcareous Alps, Austria). *Facies* 25:253–278.

921 Reijmer JJG, Palmieri P, Groen R (2012) Compositional variations in calciturbidites
922 and calcidebrites in response to sea-level fluctuations (Exuma Sound, Bahamas).
923 *Facies* 58:493–507. DOI: 10.1007/s10347-011-0291-z

924 Reijmer JJG, Mulder T, Borgomano J (2015) Carbonate slopes and gravity deposits.
925 *Sed Geol* 317:1–8. DOI: 10.1016/j.sedgeo.2014.10.011

- 926 Reuther C-D (1977) Das Namur im südlichen Kantabrischen Gebirge (Nordspanien).
927 Klustenbewegungen und Faziesdifferenzierung im Übergang Geosynklinale-
928 Orogen. Clausthaller Geol Abh 28:1–122.
- 929 Richter DK, Neuser, RD, Schreuer J, Gies H, Immenhauser A (2011) Radial-fibrous
930 calcites: A new look at an old problem. *Sed Geol* 239:23–36. DOI:
931 10.1016/j.sedgeo.2011.06.003
- 932 Rodríguez-Martínez M, Reitner J, Mas R (2010) Micro-framework reconstruction from
933 peloidal-dominated mud mounds (Viséan, SW Spain). *Facies* 56:139–15. DOI:
934 10.1007/s10347-009-0201-9
- 935 Rodríguez-Martínez M, Moreno-González I, Mas R, Reitner J (2012)
936 Paleoenvironmental reconstruction of microbial mud mounds derived boulders from
937 gravity-flow polymictic megabreccias (Visean, SW Spain). *Sed Geol* 263-264:147–
938 173. DOI:10.1016/j.sedgeo.2011.06.010
- 939 Sanz-López J (2002) Devonian and Lower Carboniferous rocks from the Cadí nappe
940 (eastern Pyrenees). In: García-López S, Bastida F (eds) *Palaeozoic conodonts from*
941 *northern Spain. Eight International Conodont Symposium held in Europe. Publ*
942 *IGME, Cuad Mus Geomin, Madrid* 1:419–438.
- 943 Sanz-López J, Melgarejo JC, Crimes PT (2000) Stratigraphy of Lower Cambrian and
944 unconformable Lower Carboniferous beds from the Valls unit (Catalonian Coastal
945 Ranges). *C R Acad Sci Paris* 330:147–153.
- 946 Sanz-López J, Blanco-Ferrera S, Sánchez de Posada LC (2004) Estratigrafía del
947 Serpukhoviense y el Bashkiriense inferior (Carbonífero) en la provincia de Pliegues
948 y Mantos Zona Cantábrica. *Geo-Temas* 6:131–134.

949 Sanz-López J, Blanco-Ferrera S, García-López S, Sánchez de Posada LC (2006) The
950 Mid-Carboniferous boundary in Northern Spain: difficulties for correlation of the
951 global stratotype and point. *Riv Ital Paleontol Stratigr* 112:3–22.

952 Sanz-López J, Blanco-Ferrera S, Sánchez de Posada LC, García-López S (2007)
953 Serpukhovian conodonts from northern Spain and their biostratigraphic application.
954 *Palaeontology* 50:883–904.

955 Sanz-López J, Blanco-Ferrera S, Sánchez de Posada LC (2013) Conodont
956 chronostratigraphic resolution and *Declinognathodus* evolution close to the Mid-
957 Carboniferous Boundary in the Barcaliente Formation type section (NW Spain).
958 *Lethaia* 46:438–453. DOI: 10.1111/let.12021

959 Sanz-López J, Cózar P, Blanco-Ferrera S (2018) Discovery of a Mississippian-early
960 Bashkirian carbonate platform coeval with condensed cephalopod limestone
961 sedimentation in NW Spain. *Geol J* 53:2532–2557. DOI: 10.1002/gj.3087

962 Schönlaub HP, Histon K (2000) The Palaeozoic evolution of the Alps. *Mitt Österr Geol*
963 *Ges* 92:15–24.

964 Shanmugam G (2017) Contourites: physical oceanography, process sedimentology, and
965 petroleum geology. *Pet Explor Dev* 44:183–216.

966 Somerville ID, Strogon P, Jones, GLI, Somerville HEA (1996) Late Viséan buildups at
967 Kingscourt, Ireland: possible precursors of Upper Carboniferous bioherms. In:
968 Strogon P, Somerville, ID, Jones GLI (eds), *Recent advances in Lower*
969 *Carboniferous Geology*. Geological Society Special Publication No. 107, London,
970 pp. 127–144.

971 Stanley DJ (1988) Turbidites reworked by bottom currents: Upper Cretaceous examples
972 from St. Croix, U.S. Virgin Islands. *Smithson Contrib Mar Sci* 33:1–79.

973 Sudar MN, Novak M, Korn D., Jovanović D (2018) Conodont biostratigraphy and
974 microfacies of the Late Devonian to Mississippian Milivojevića Kamenjar section
975 (Družetić, NW Serbia). Bull Geosci 93: 163–183. DOI: 10.3140/bull.geosci.1690
976 Tucker ME (1974) Sedimentology of Palaeozoic pelagic limestones: The Devonian
977 Griotte (Southern France) and Cephalopodenkalk (Germany). Spec Publs Int Ass
978 Sediment 1: 71–92.
979 Tucker ME (2003) Mixed clastic-carbonate cycles and sequences: Quaternary of Egypt
980 and Carboniferous of England. Geol Croat 56:19–37.
981 Vachard D, Cózar P (2010) An attempt of classification of the Palaeozoic incertae sedis
982 Algospongia. Rev Esp Micropaleontol 42:129–241.
983 Vachard D, Cózar P, Aretz M, Izart A (2016) Late Viséan-early Serpukhovian
984 cyanobacteria and algae from the Montagne Noire (France); taxonomy and
985 biostratigraphy. Bull Geosci 91:433–466. DOI: 10.3140/bull.geosci.1613
986 Vachard D, Izart A, Cózar, P (2017) Mississippian (middle Tournaisian-late
987 Serpukhovian) lithostratigraphic and tectonosedimentary units of the southeastern
988 Montagne Noire (Hérault, France). Geol Fr 1:47–88.
989 Wendt J, Aigner T (1985) Facies patterns and depositional environments of Palaeozoic
990 cephalopod limestones. Sed Geol 44:263–300.
991 Wright VP (1992) A revised classification of limestones. Sed Geol 76:177–185.
992

993 **Figure Captions**

994

995 **Table 1** Lithofacies of the Valdediezma Limestone.

996

997 **Fig. 1** Location of the study area and the Valdediezma Limestone (black) within the
998 Cantabrian Zone and the different tectonostratigraphic units or provinces, particularly
999 them the Picos de Europa Province. (1) Millaró section, (2) Alba Syncline.

1000

1001 **Fig. 2a** The main lithostratigraphic units from the Famennian (Devonian) to the
1002 Moscovian (Carboniferous) in the Picos de Europa Province (Aliseda-Cabrones-Vegas
1003 de Sotres and Tejo tectonic units) in comparison with those typical of the Cantabrian
1004 Zone. **b** Tectonics subunits distinguished in the Tejo unit and location of the studied
1005 stratigraphic sections: (I) Argaña, (II) road to Sotres, el Bosque-Navayu, (III)
1006 Valdediezma valley, (IV) Jitu l'Escarandi, (V) Cheese Cave in the Sobra valley, (VI)
1007 road from the Jitu l'Escarandi to the Casetón de Andara, (VII) Pompedrei Bridge, (VIII)
1008 La Hermida, (IX) Mesa Sin Pan, (X) Cueto de los Senderos, (XI) Vegas de Sotres.

1009

1010 **Fig. 3** Stratigraphic log of the Valdediezma Formation at the Valdediezma-Jitu
1011 l'Escarandi section (Saigu subunit) on the left side showing the recognized facies (1 to
1012 16 as in Table 1). Abbreviations: mc microbial, m mudstone and shales, m-w mudstone-
1013 wackestone, w-p wackestone packstone, g grainstone, r rudstone and floatstone. On the
1014 right side, thin-section photos of the main microfacies (scale bar in the pictures = 2 mm;
1015 way-up is to the photo top). **a** Micropeloidal to peloidal (upper part) cement-supported
1016 texture (Facies F2). In the middle, a large fenestral cavity with RFC and poorly
1017 developed blocky cement. *Terebella*-like tube (t), faecal pellets (p), crinoids (c) and

1018 ostracods are observed, Pc4946. **b** Bioclastic cement-supported texture (Facies F5) rich
1019 in fenestellids bryozoans (f), brachiopods (b) and crinoids (c), Pc4285. **c** Bioclastic
1020 matrix-supported passing into bioclastic cement-supported texture (Facies F5 and F6).
1021 Contact between both textures is gradual (particularly rich in foraminifers) and it is
1022 oblique the upper top of the bed, Pc4975. **d** Mound-intermound facies alternation, with
1023 peloidal matrix-supported textures (p) (Facies F3) veneered by a cyanobacterial crust
1024 (cy). Above, a bioclastic grainstone (g) (Facies F13) is filling the palaeorelief of the
1025 microbial facies, with common oncoids (o), passing into the upper part to micropeloidal
1026 textures (m) with brachiopods (b) and incrusting foraminifers (*Pseudolituotuba gravata*,
1027 pg), Pc4976. **e** Poorly sorted and fragmented wackestone (Facies F9) containing
1028 molluscs with micritic rims around the bioclasts, Pc4960. **f** Bioturbated mudstone-
1029 wackestone (Facies F8) rich in calcispheres, foraminifers and ostracods, Pc4957. **g**
1030 *Calcifolium* grainstone (Facies F13), Pc4953. **h** Ooids and cortoids in grainstone (Facies
1031 F14) in the intermound facies. Foraminifera and dasycladales are common, Pc4971.

1032

1033 **Fig. 4a** Two microbial mounds (base and top highlighted with dotted lines) in the lower
1034 part of the Valdediezma Limestone close to the trail between the Jitu l'Escarandi and
1035 Bejes (Valdediezma valley). **b** Lower part of the Valdediezma Limestone (interval I1),
1036 where one buildup is highlighted. The base of the picture corresponds to sample Pc
1037 4948, and the top of the hill corresponds to sample Pc 5967 (Fig. 3). **c** Upper part of the
1038 Valdediezma section, at Jitu l'Escarandi with laterally amalgamated mounds (interval
1039 I5, corresponds to samples Pc 5073 to Pc 5935), solid line at the base corresponds to a
1040 fault; bioclastic facies and microbial mounds in interval I6 (equivalent to samples Pc
1041 4951 to Pc 4957), most of the bioclastic facies does not crop out apart from the road
1042 section, and most of the observed limestones in this interval correspond to microbial

1043 mounds. Microbial mounds are almost absent in the interval I7 (upper part of the
1044 sections in Fig. 3).

1045

1046 **Fig. 5** Stratigraphic log of the Pompedrei Bridge section (Las Llamas-Bejes subunit) on
1047 the left side, showing the recognized facies (1 to 16 as in Table 1). Abbreviations as in
1048 Fig. 3. On the right side, thin-section photos of the main facies (scale bar = 1 mm; way-
1049 up to the top of the picture). Dark arrows are the samples for foraminifers and
1050 sedimentology. **a** Medium-grained well sorted packstone (Facies F11), Valdediezma
1051 Limestone, Pc5108. **b** Microsequences of wackestone to packstone (Facies F12)
1052 Valdediezma Limestone, Pc5105. **c** Typical bioturbated mudstones to wackestone
1053 (Facies F8) of the Millaró Member, Pc5009. **d** Bioclastic-intraclastic packstone
1054 intercalated (Facies F11) in the Millaró Member, note that foraminifers and
1055 *Praedonezella* (most of the pale grey small clast in the matrix) are common, Pc5118. **e**
1056 Cement-supported micropeloidal limestone (Facies F2) with common small stromatactis
1057 cavities with a thin rim of radiaxial cement and blocky spar at the base of the
1058 Barcaliente Formation, Pc5119. **f** Bioclastic packstone-wackestone (Facies F10) layer
1059 with crinoids and *Calcifolium* (c) within the lower part of the Barcaliente Formation,
1060 Pc5120. **g** Laminated micrites (Facies F7) with spicules in the lower part, typical of the
1061 Barcaliente Formation, and an upper layer (Facies F8) displaying a finning-upward
1062 sequence (with spicules, ostracods and foraminifers), Pc5121. **h** Recrystallized
1063 cementstone (Facies F1) with ghosts of algae and bioclasts with micrite coatings,
1064 Valdediezma Limestone, Pc5123.

1065

1066 **Fig. 6a** Stratigraphic section of the Mesa Sin Pan section (Mesa Sin Pan subunit). Dark
1067 arrows indicate the position of foraminifers and sedimentology samples, white arrows

1068 mark position of conodont samples. **b** Stratigraphic section of the Argaña section
1069 containing the Alba and Valdediezma formations (Varera subunit). **c** Stratigraphic logs
1070 of the Alba Formation and the interbedded Valdediezma Limestone in the Cueto de los
1071 Senderos section, in the Aliseda-Cabrones-Vegas de Sotres unit. Abbreviations: BAS.
1072 Bashkirian, C Canalón Member, G Gorgera Member, Mill. Millaró Member, Prot.
1073 Protvian. S. Steshevian, Taru. Tarussian, Vozne. Voznesenian.
1074

1075 **Fig. 7** Stratigraphic log of the Vegas de Sotres section (Aliseda-Cabrones-Vegas de
1076 Sotres unit) on left side, showing the recognized microfacies (F7 to F16 as in Table 1).
1077 Abbreviations: mc microbial, m mudstone and shales, m-w mudstone-wackestone, w-p
1078 wackestone-packstone, g grainstone, r rudstone, floatstone and Bar Barcaliente. Note
1079 that the same facies are in pink and grey colours. On the right side, thin section
1080 photographs of the main microfacies (scale bar = 2 mm; way-up to the top of the
1081 picture). **a** Radiolarian mudstone to wackestone (right), ferromanganese concentrations
1082 in stylolites (Facies F7), Canalón Member, VSF-101. **b** Bioturbated wackestones with
1083 ostracods and sponge spicules, ostracods mark a poorly defined low-angle cross-
1084 lamination (Facies F8), Canalón Member, VSF-103. **c** Wackestone to packstone in
1085 coarsening-upward sequence (Facies F12), Valdediezma Limestone, VSF-14g. **d**
1086 Mudstone (m) at the base with bioclastic wackestone (w)-packstone (p) coarsening-
1087 upward (Facies F12). The upper wackestone is separated by another erosive surface,
1088 Valdediezma Limestone, lower part of VSF-18 (see also F). **e** Microsequence passing
1089 from wackestone to grainstone (Facies F12), Valdediezma Limestone, VSF-7. **f** Upper
1090 part of the sequence in D, with a grainstone (Facies F12) showing a distinct erosive
1091 surface separating it from a packstone containing micrite intraclasts. Valdediezma
1092 Limestone, VSF-18. **g** Packstone passing into wackestone in a fining-upward

1093 microsequence (Facies F12), Valdediezma Limestone, VSF-4e. **h** Rudstone (Facies
1094 F16) composed of intraclasts of grainstone (g), packstone (p) to mudstone with
1095 radiolarians (m) in a wackestone matrix with many small intraclasts, Valdediezma
1096 Limestone, VSC-6A.

1097

1098 **Fig. 8** Correlation proposed for the different sections studied in the Tejo unit between
1099 the upper Tournaisian and the lower Bashkirian (location of sections in Fig. 2), and two
1100 simplified sections from the western Cantabrian Zone (location of sections in Fig. 1).
1101 The upper Tournaisian to middle Viséan is not observed in the Valdediezma-Jitu
1102 l'Escarandi-Cheese Cave. Absolute ages based on Davydov et al. (2012). Compare the
1103 stratigraphic thickness below and above the black correlation line in the upper
1104 Serpukhovian. They accumulated during a time interval some eleven times longer
1105 below (Viséan-Serpukhovian, from 346.7 to 324.5 Ma) than above (Serpukhovian-early
1106 Bashkirian, from 324.5 to 322.5 Ma).

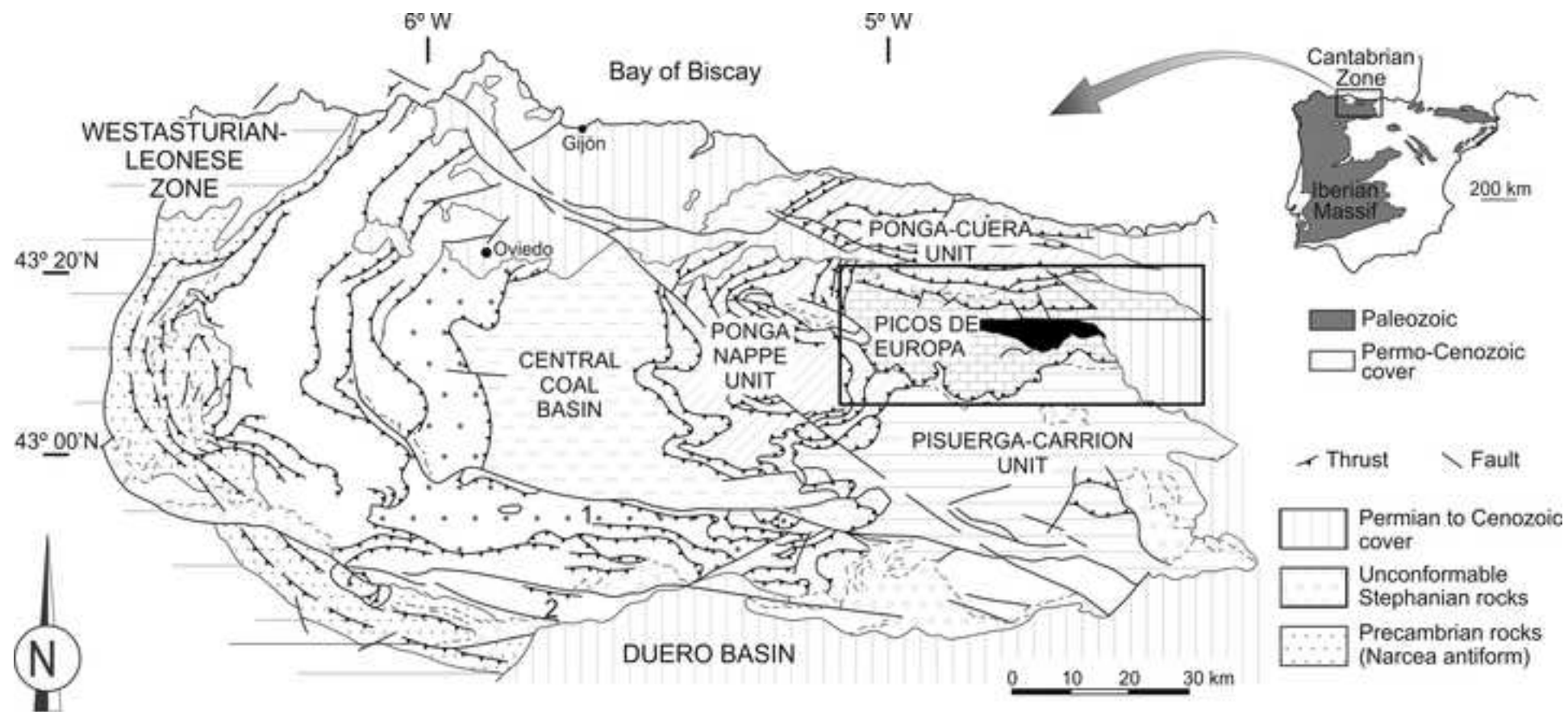
1107

1108 **Fig. 9a** Distribution of the Gorgera and Lavandera members of the Alba Formation
1109 indicating sedimentary highs (shown as numbers) and troughs in the lower-middle
1110 Viséan of the Cantabrian Mountains. (I) lacking or thin Lavandera Member, or pelagic
1111 platform, (II) Lavandera Member occurs, (III) Gorgera Member lacking in the Palentine
1112 nappes, originally rooted southwards (arrow), (IV) Valdediezma Limestone. **b** Cross-
1113 section with the interpreted model of the subdivided basin without scale.

1114

1115 **Fig. 10a** Schematic map of the north branch of the Ponga Nappe (Ponga-Cuera) and the
1116 Picos de Europa provinces modified from Bahamonde et al. (2007, 2008) showing the
1117 current geographic extent of the depositional zones for the carbonate platform of the

1118 Valdeteja and Picos de Europa formations. The Valdediezma Limestone is located in
1119 the core of the internal area of the Picos de Europa province. The direction and sense for
1120 the progradation of the Pennsylvanian carbonate and Valdediezma platforms is
1121 indicated (white arrows). **b** The correlation diagram shows the temporal relation of the
1122 Valdediezma Limestone and the differential sedimentation and subsidence with respect
1123 to the Alba and Barcaliente formations (absolute ages according to Davydov et al.,
1124 2012, are indicating lower sedimentation rate for the older rocks in the external area).
1125 The uplift and erosion of the Valdediezma platform is indicated by a sedimentary hiatus
1126 (vertical lines and arrows). The burial of the Valdediezma platform by strata of the
1127 uppermost part of the Picos de Europa Formation was due to the extended subsidence of
1128 the Picos de Europa province (Gamonedo-Cabrales, Central and Frontal units) as
1129 consequence of the emplacement of the frontal thrust sheets of the Ponga Nappe
1130 Province (Sierra del Cuera).

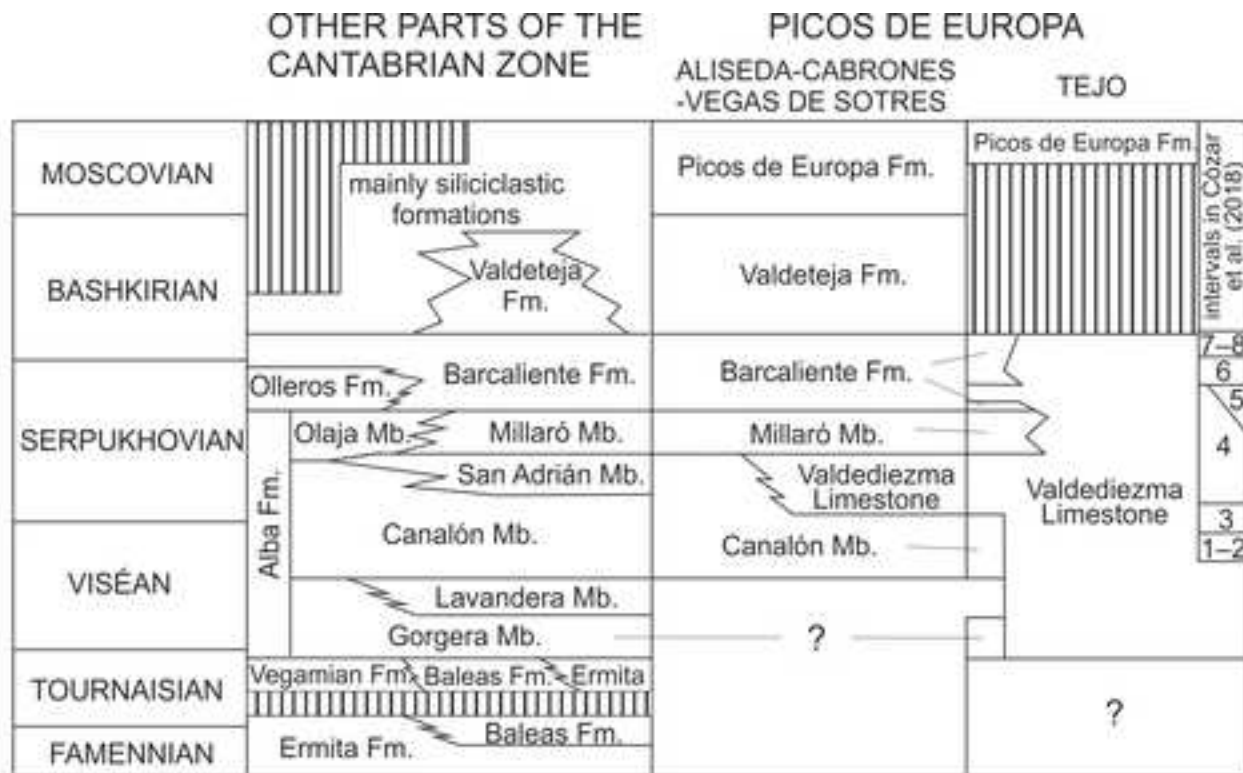


PALAEZOIC ROCKS IN THE MAJOR THRUST UNITS OF THE CANTABRIAN ZONE

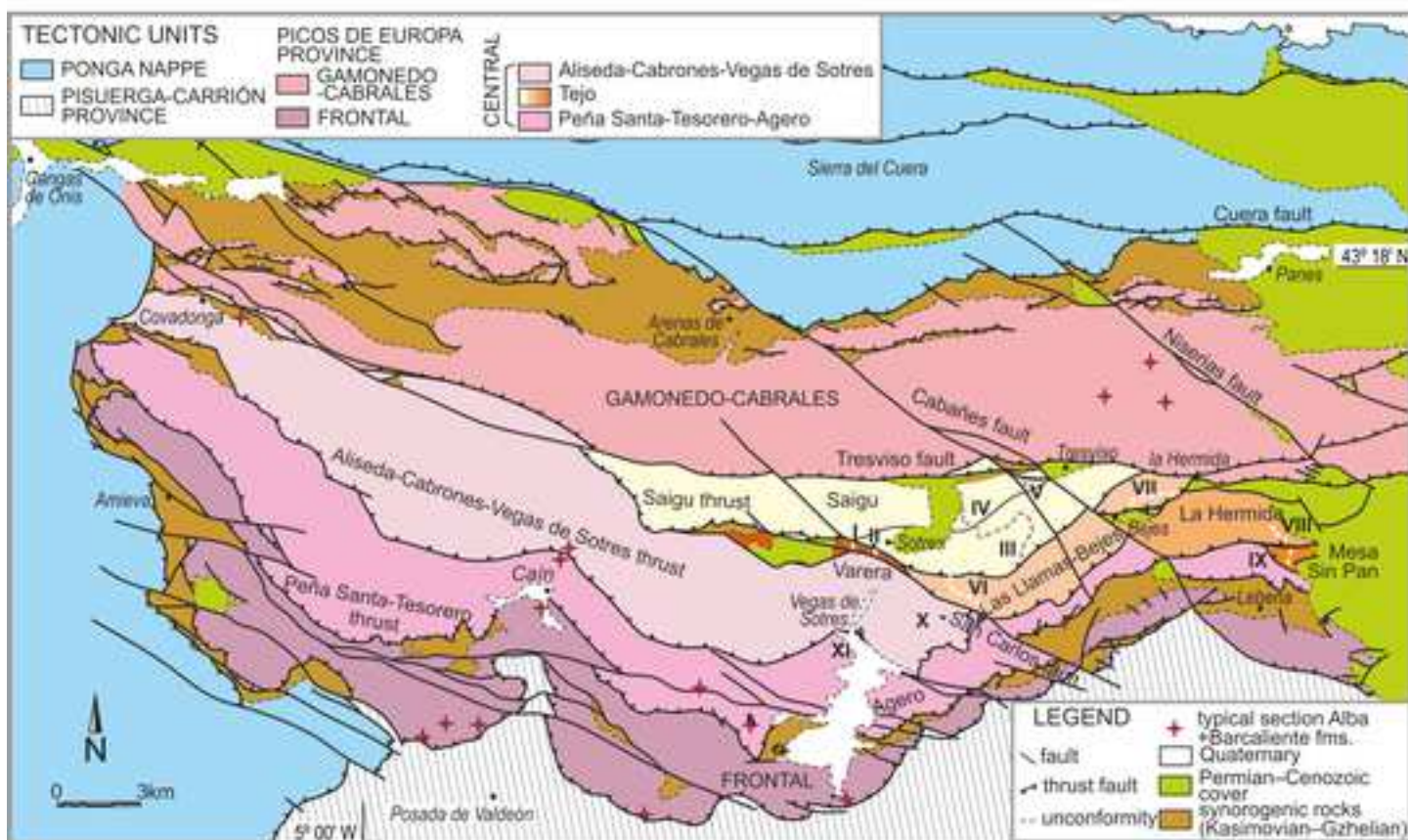
BODÓN-PONGA UNIT



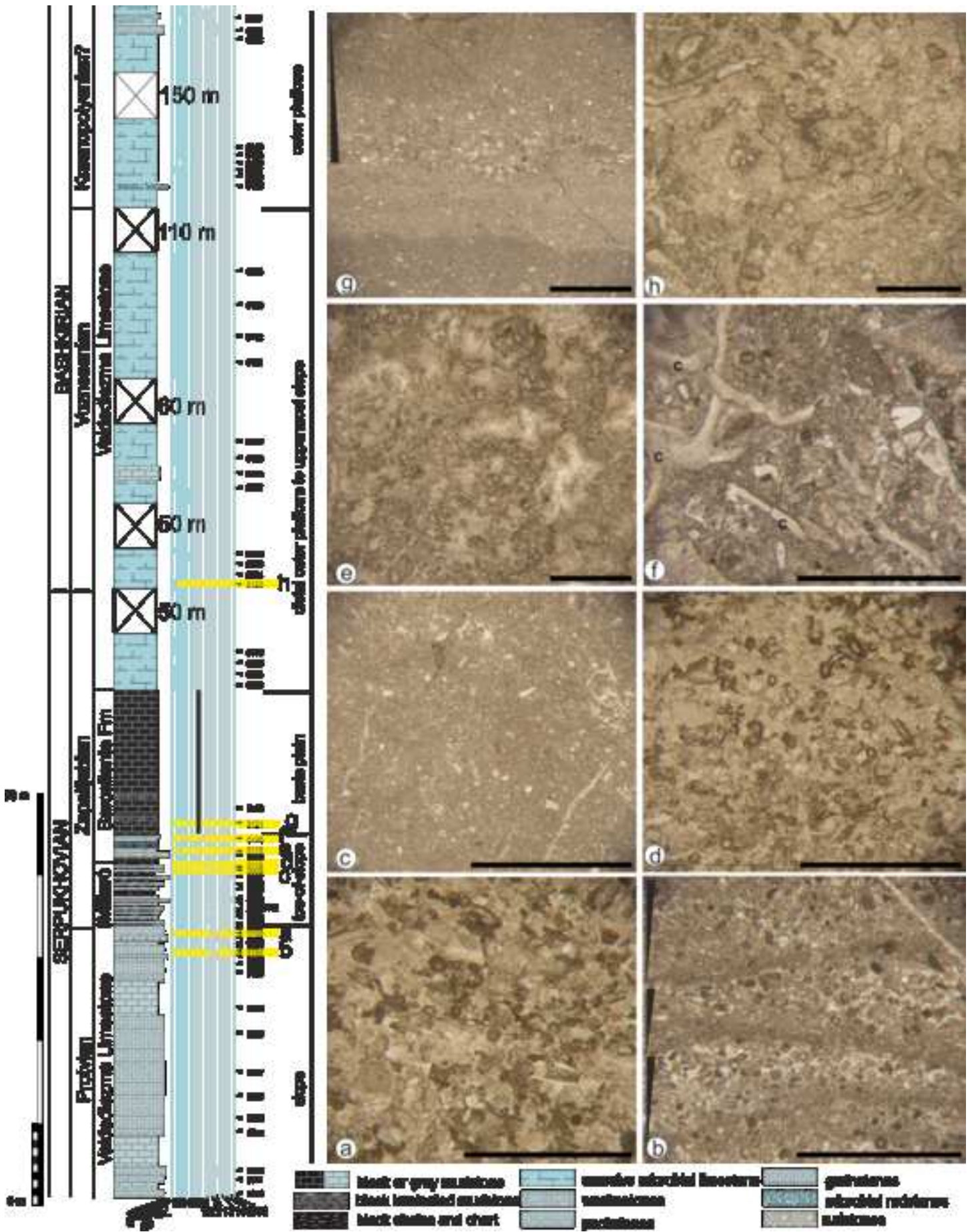
a



b







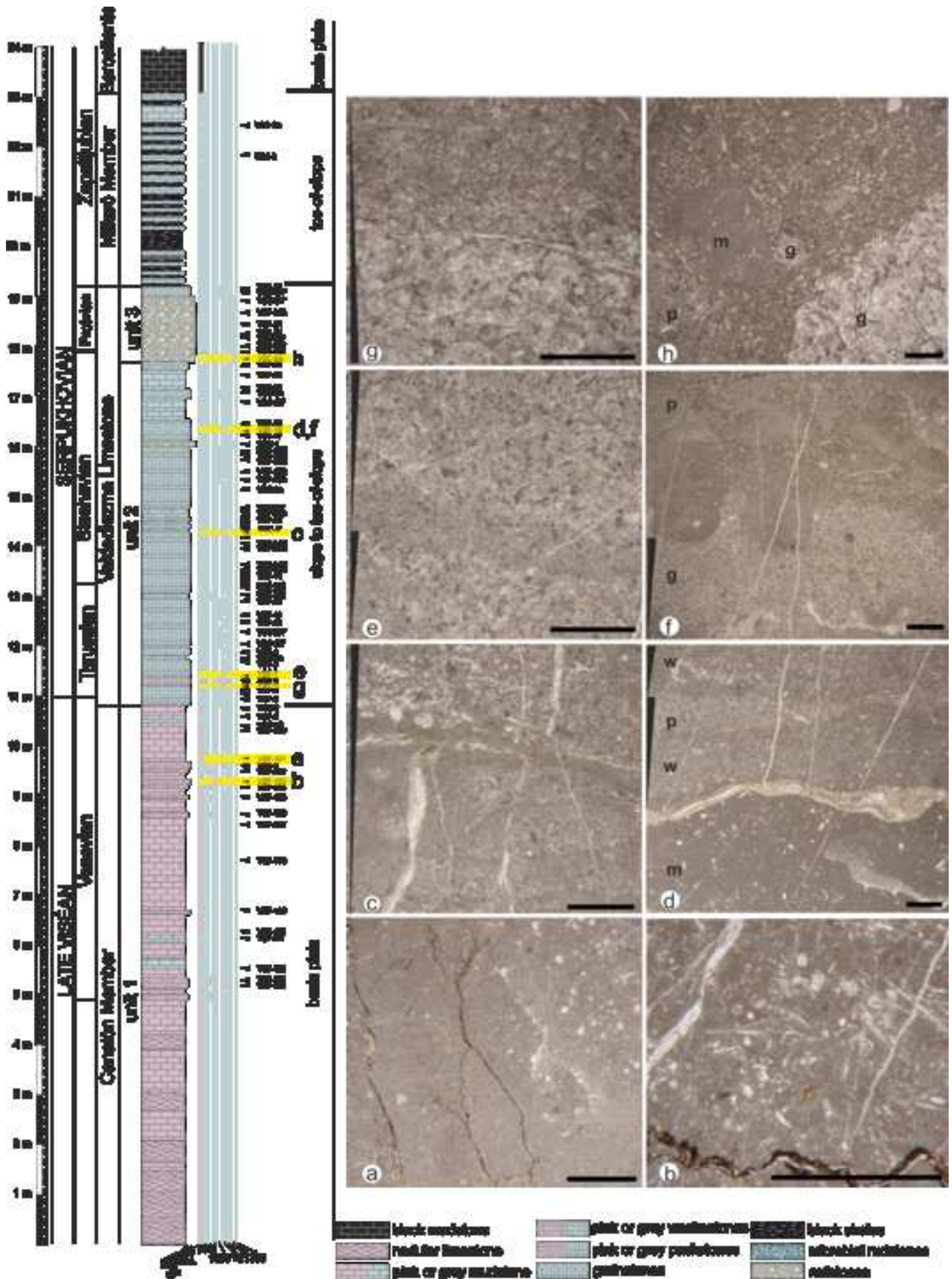
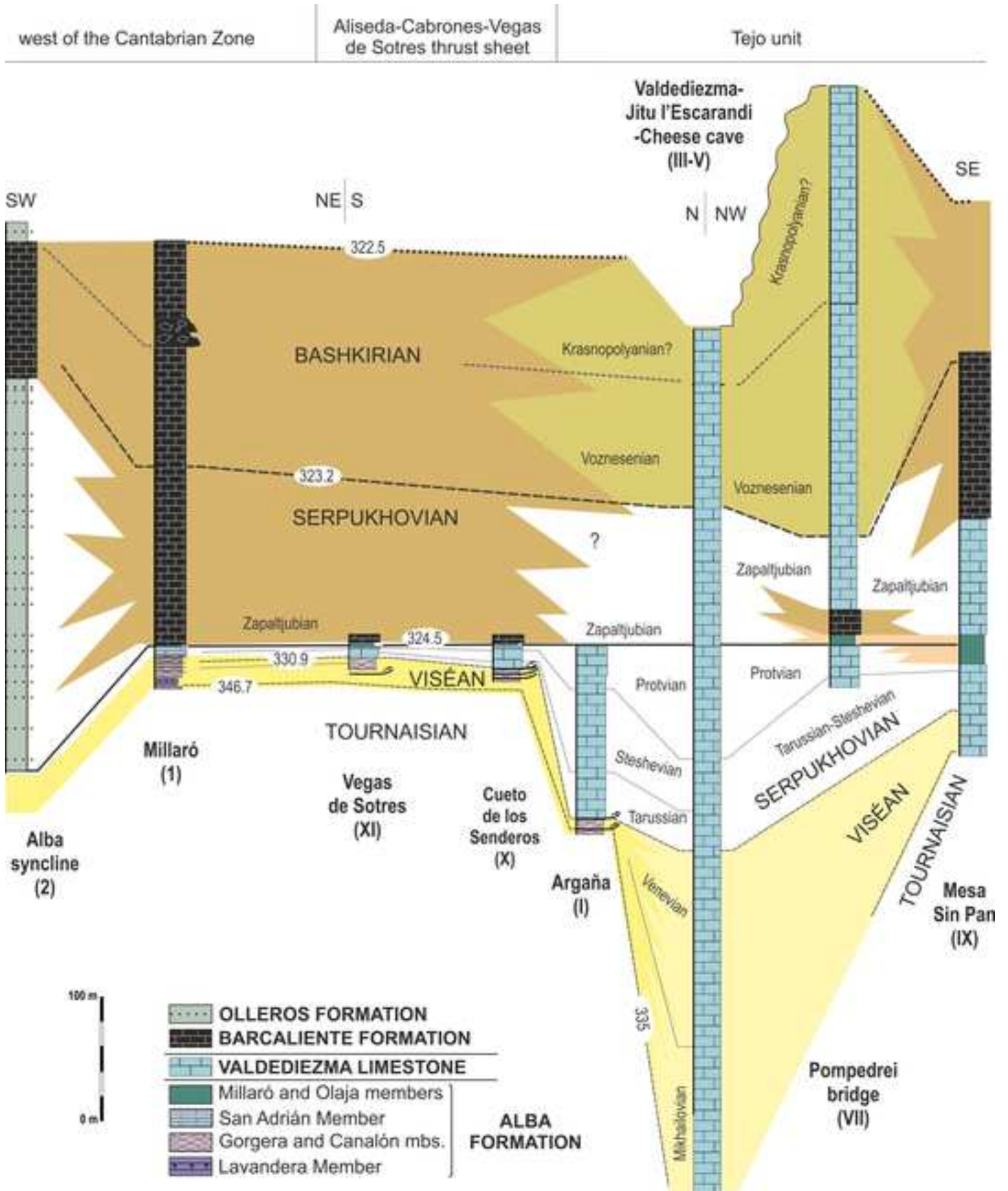
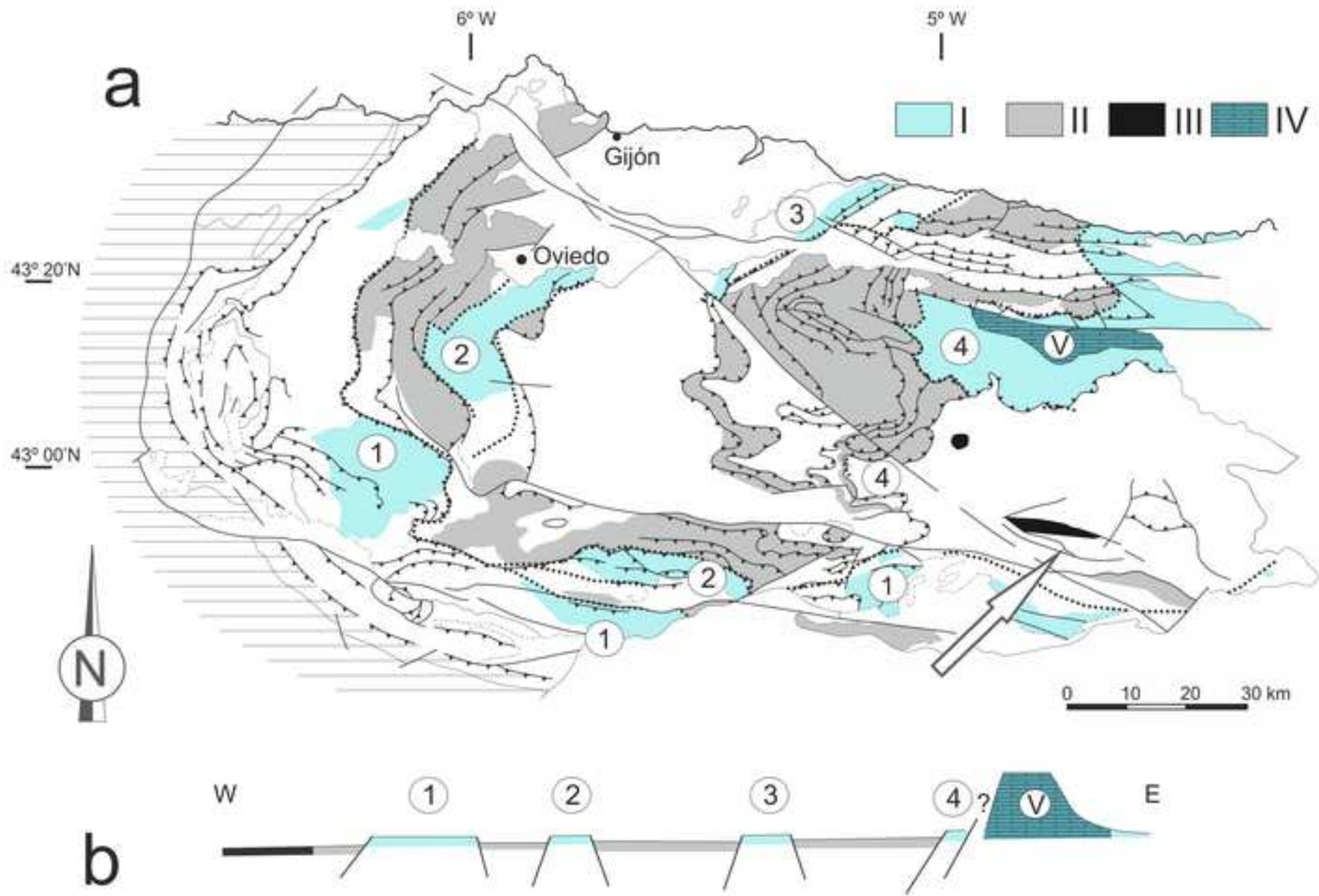


Figure 8

[Click here to access/download;Figure;Fig8 BlancoFerrera.tif](#)





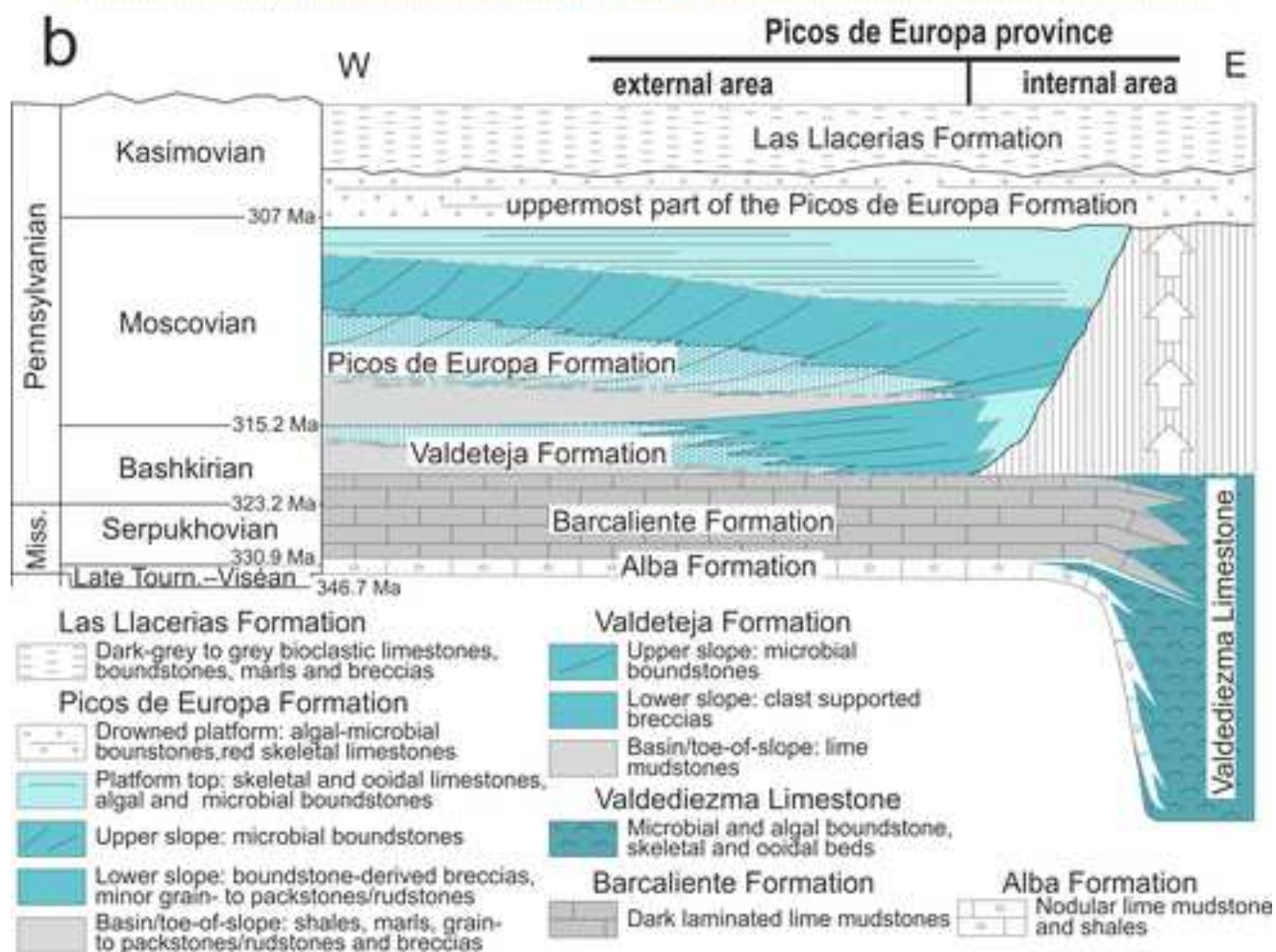
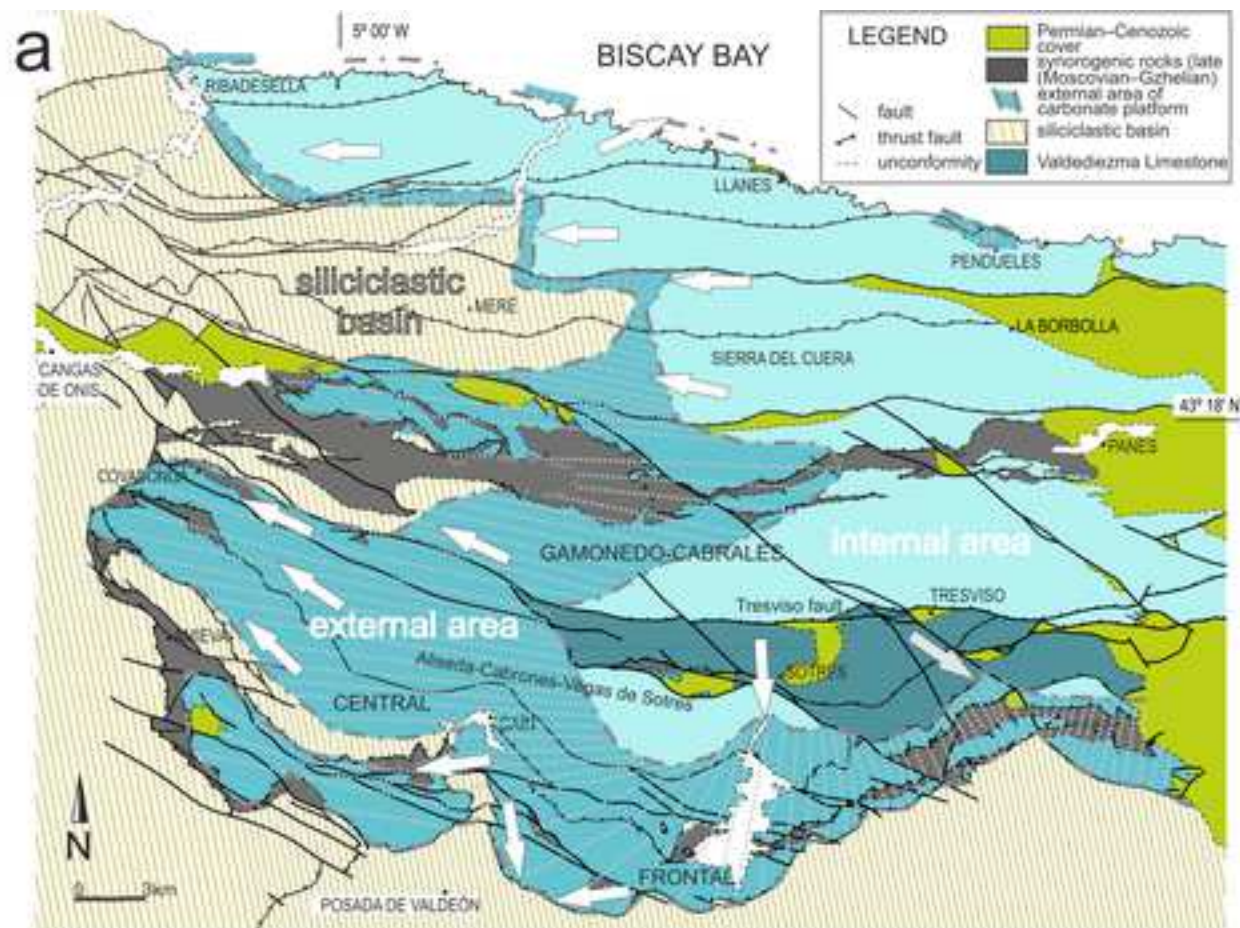


Table 1

	Facies	Cement and matrix	Allochlems	Bioclasts	Microbial transitions	Microbial growths
MICROBIAL FACIES	F1 Cemenstone	cements > 40% (common RFC filling fenestrae, rare blocky cement in large fenestrae), automicrite 0–60% (micropeloids <40%, peloids <15%)	low to moderate content (0–55%); rare grapestones, oncoids, cortoids and abundant lithoclasts (up to 45%)	moderate to low, varying from 0% to 35%. Abundant: fenestellids, crinoids, brachiopods and ostracods. Commonly present: <i>Praedonezella</i> , <i>Calcifolium</i> , cyanobacteria. Rare: calcispheres, tabulate corals	commonly to peloidal cement-supported texture, and more rarely to matrix-supported texture. Exceptional transitions to the bioclastic, micritic facies and grainstones	Predominantly laminar growth, exceptionally with lateral changes of facies and patchy distribution. Moderate abundance of fenestrae (half of the samples). Occasional development of firmgrounds.
	F2 Cement-supported	cements 30–60% (common RFC and blocky filling fenestrae), automicrites 0–45% (micropeloids < 30%, peloids <20%)	moderate content (<35%), common grapestone (<30%) and lithoclasts (<20%), and rare ooids and oncoids	moderate to low (5 to 25%). Abundant crinoids, brachiopods, fenestellids, ostracods, foraminifers, molluscs. Commonly present cyanobacteria, <i>Praedonezella</i> and <i>Calcifolium</i> ; rare <i>Clara crusta</i> , <i>Donezella</i> , <i>Wheteredella</i> , encrusting and trepostomate bryozoans, rugose corals and sponges	commonly to bioclastic cement-supported and cemenstone facies, and rarely to peloid matrix-supported texture	Predominant laminar and secondary patchy distribution of peloids and cements, with abundant fenestrae.
	F3 Peloidal matrix-supported	cement 10–30% (common RFC and blocky filling fenestrae), automicrites 10% to 70% (micropeloids 0–50%, peloids 0–40%)	high content (up to 50%), common grapestones, lithoclasts, ooids, oncoids, and cortoids	moderate (5–40%). Abundant brachiopods, foraminifers, crinoids, <i>Calcifolium</i> , <i>Praedonezella</i> , calcispheres and cyanobacteria. Commonly present are ostracods and molluscs. Rare rugose corals, sponge spicules, trepostomate and encrusting bryozoans, Aphralysiacean, <i>Ungarella</i> , <i>Clara crusta</i> and dasycladales	rare to peloidal cement-supported and to cemenstones and micritic facies, as well as with wackestones and grainstones	Laminar, patchy and domical growth of the facies, with abundant small fenestrae. Rare development of hardgrounds and firmgrounds
	F4 Matrix-supported	cement 0–20% (rare RFC and blocky filling fenestrae), automicrites 10% to 70% (micropeloids 0–30%, peloids 0–45%)	low content (0–5%), with rare lithoclasts and grapestones	high content (30–50%). Abundant crinoids, brachiopods, <i>Praedonezella</i> , and <i>Fasciella</i> . Commonly present molluscs and cyanobacteria. Rare tabulate and rugose corals, sponge spicules, ostracods, encrusting and fenestellid bryozoans and <i>Calcifolium</i>	Commonly to the bioclastic cement-supported and matrix-supported textures, rarely to mudstones-wackestone, peloidal matrix-supported, bioclastic matrix-supported, and exceptionally to cemenstone textures	laminar growths, with very small fenestrae, filled by polymuds.
	F5 Matrix-supported	cement 20–60% (common blocky and rare RFC filling fenestrae), automicrites 0–40% (micropeloids 0–20%, peloids 0–30%)	moderate (<30%), with common grapestones, lithoclasts and ooids, and more rarely oncoids and cortoids	high content (15–70%). Abundant crinoids, foraminifers, brachiopods, <i>Calcifolium</i> , <i>Praedonezella</i> , <i>Fasciella</i> , fenestellids and molluscs. Commonly present are sponges, Dasycladales, cyanobacteria, calcispheres, aouggalids, encrusting bryozoans. Rare ostracods, gastropods and rugose corals	commonly to the bioclastic matrix-supported and micritic facies and rarely to cemenstones and grainstones	laminar, patchy and domical growths. Common developments of fenestrae. Occurrence of firmgrounds.
	F6 Matrix-supported	cement 3–40% (rare blocky and RFC filling fenestrae), automicrites 0–40% (micropeloids 0–20%, peloids 0–15%)	moderate to high (<40%), with common grapestones, lithoclasts and ooids, and more rarely oncoids and cortoids	high content (40–80%). Abundant brachiopods, <i>Calcifolium</i> , cyanobacteria, <i>Praedonezella</i> , crinoids. Commonly present are rugose corals, <i>Fasciella</i> , <i>Clara crusta</i> , Dasycladales and ostracods. Rare Aphralysiacean, calcispheres, fenestellids, molluscs and sponges	commonly to peloidal matrix-supported and cement-supported and micritic facies, more rarely to cemenstone and grainstone	Predominantly laminar growths, rare fenestrae and rare firmgrounds.
Predominantly NON-MICROBIAL FACIES	F7 Mudstone	cement absent, automicrites absent, allomicrite 55–95%	rare lithoclasts	low 5 to 20% exceptionally 40%. Abundant ostracods, sponge spicules, crinoids, foraminifers. Commonly present are radiolarians, calcispheres. Rare <i>Praedonezella</i> , brachiopods, and trilobites	rarely to packstone in coarsening-upward sequences.	
	F8 Mudstone-wackestone	cement rare (<5 in one sample), allomicrite 60–85%. Automicrites rarely present, but with high percentages (10–40%)	low content, rarely lithoclasts and oncoids	low to moderate (10–40%). Abundant crinoids, <i>Donezella</i> , ostracods and calcispheres. Commonly present are foraminifers and brachiopods. Rare <i>Praedonezella</i> , sponge spicules, tabulate corals, fenestellid and encrusting bryozoans	rare to micritic facies with grumular structures.	
	F9 Wackestone	cement low (2–30%) in a few samples. Allomicrite <65%. Automicrites commonly present, up to 40%	low content, rare lithoclasts and oncoids	moderate (30–50%). Abundant crinoids, <i>Praedonezella</i> , <i>Calcifolium</i> , brachiopods, calcispheres, foraminifers, <i>Fasciella</i> , <i>Donezella</i> and molluscs. Commonly present spongy spicules. Rare gastropods, cyanobacteria and dasycladales	commonly to micritic and peloidal matrix-supported facies.	
	F10 Poorly to moderate sorted packstone	cement in half of the samples in low percentages (10–20%). Allomicrite 5–40%. Automicrites in two samples, 20–50%	high content, with abundant lithoclasts (in samples up to 30%), ooids and grapestones.	high (50–60%), with abundant <i>Calcifolium</i> , crinoids, <i>Praedonezella</i> and foraminifers. Commonly present are <i>Donezella</i> , ostracods, calcispheres and tabulate corals. Rare Aphralysiacean, fenestellids, brachiopods and rugose corals	rarely to bioclastic matrix-supported facies.	
	F11 Well-sorted packstone	cement present in half of the samples, 10–20%	high content, restricted to lithoclasts (<40%)	moderate to high (30–70%), mostly restricted to crinoids, <i>Praedonezella</i> and fenestellids. Commonly present ostracods, calcispheres, foraminifers, <i>Calcifolium</i> and <i>Fasciella</i> . Rare brachiopods and sponge spicules	none.	
	F12 graded mudstone to packstone	cement 0–30%	low content, restricted to small intraclasts, 0–20%	moderate to high (20–60%), mostly restricted to crinoids, ostracods, calcispheres, sponge spicules and foraminifers. Rare <i>Kamaenella</i> , molluscs and fenestellids	none.	
	F13 Bioclastic grainstone	cement 25–60%. Allomicrite absent. Automicrite 10–30%	high content, with percentage between 20% and 60%, commonly lithoclasts, ooids, cortoids and grapestones	moderate to high (<60%). Abundant <i>Calcifolium</i> , crinoids, brachiopods, foraminifers, calcispheres and <i>Praedonezella</i> . Commonly present are encrusting bryozoans and sponges. Rare molluscs, Dasycladales, <i>Clara crusta</i> , Aphralysiaceans, calcimicrobes, ostracods and rugose corals	Rare to the bioclastic and peloidal matrix-supported, micritic and cemenstone facies.	
	F14 Ooidal grainstone	cement 20–50%. Allomicrite absent. Automicrites <10%	high content, mostly ooids (>30%), but also some lithoclasts, cortoids, and grapestones	moderate to low (<25%). Abundant crinoids, brachiopods, molluscs. Presence of Dasycladales, foraminifers and calcimicrobes	exceptional transitions to bioclastic matrix-supported facies.	
F15 Microbial rudstone-floatstone	allomicrite 15–35%	high content, lithoclasts 50x90%, all composed only by microbial clasts	rare, exclusively crinoids (10–20%) and rugose corals (10%).			
F16 Rudstone	allomicrite 5–20%.	high content, lithoclasts 80–90%, composed of bioclastic grainstone-packstones, laminated micrites, and rarely microbial clasts.	usually absent.			